

# Crystalline Multi-Metallic Compounds as Host Materials in Cathode for Lithium–Sulfur Batteries

Yi-Cheng Jiang, Hafiz Muhammad Umair Arshad, Hao-Jie Li, Sheng Liu, Guo-Ran Li,\* and Xue-Ping Gao\*

Lithium–sulfur (Li–S) battery is one of the most promising next-generation rechargeable batteries. Lots of fundamental research has been done for the problems during cycling like capacity fading and columbic efficiency reducing owing to severe diffusion and migration of polysulfide intermediates. In the early stage, a wide variety of carbon materials are used as host materials for sulfur to enhance electrical conductivity and adsorb soluble polysulfides. Beyond carbon materials, metal based polar compounds are introduced as host materials for sulfur because of their strong catalytic activity and adsorption ability to suppress the shuttle effect. In addition, relatively high density of metal compounds is helpful for increasing volumetric energy density of Li–S batteries. This review focuses on crystalline multi-metal compounds as host materials in sulfur cathodes. The multi-metal compounds involve not only transition metal composite oxides with specific crystalline structures, binary metal chalcogenides, double or complex salts, but also the metal compounds doped or partially substituted by other metal ions. Generally, for the multi-metal compounds, microstructure and morphologies in micro–nano scale are very significant for mass transfer in electrodes; moreover, adsorption and catalytic ability for polysulfides make fast kinetics in the electrode processes.

material realizing their full capacity is difficult in Li–S cells.<sup>[2,3]</sup> The low utilization of active material results due to the insulating nature of sulfur that impedes the electron transfer during electrochemical reactions, which stems from low conductivity of sulfur.<sup>[4]</sup> Sulfur with high resistances ( $\approx 10^{-30}$  S cm<sup>-1</sup>) experiences a series of structural and morphological changes during charge–discharge process which involve the formation of high order soluble intermediates lithium polysulfides (Li<sub>2</sub>S<sub>x</sub>, 8 < x < 3) (LiPSs) and low order insoluble sulfides (Li<sub>2</sub>S<sub>2</sub>/Li<sub>2</sub>S) in the liquid electrolyte, resulting in severe capacity fade because of unstable electrochemical contact within sulfur electrodes. The higher order soluble intermediates lithium polysulfides ions formed shuttle between the anode and the cathode which reduce energy output that lead to a rapid decline in columbic efficiency.<sup>[5]</sup> Furthermore, the conversion of sulfur to LiPSs evolves not only structural and morpho-

## 1. Introduction

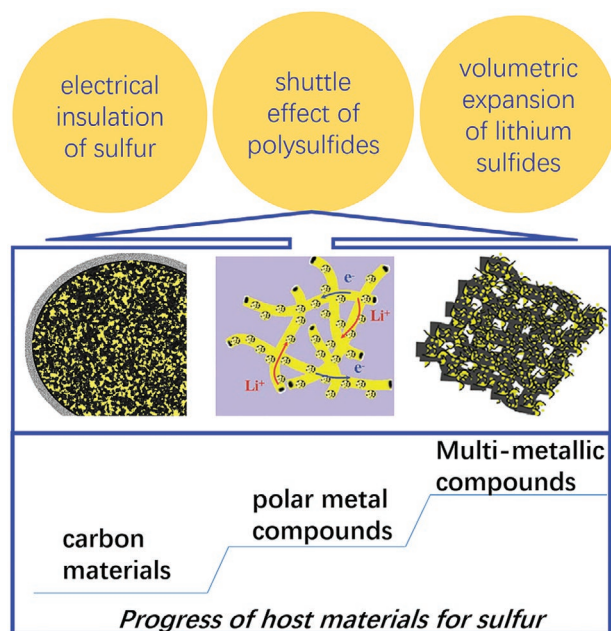
Development of portable electronics and electric vehicles yearns for rechargeable batteries with high energy density. Lithium-ion batteries based on the insertion mechanism usually have energy density of less than 200 Wh kg<sup>-1</sup>. Lithium–sulfur batteries offer a theoretical energy density of 2600 Wh kg<sup>-1</sup>, and currently a practical energy density up to 500–600 Wh kg<sup>-1</sup> is available, which is about thrice as high as that of lithium-ion batteries.<sup>[1]</sup> Even though sulfur cathodes have high theoretical energy density however, there are several challenges for practical application because of physical and chemical properties of sulfur, polysulfide intermediates, and great complexity in the electrode processes that lead to low utilization of the active

logical changes but also repetitive dissolution and deposition, resulting in passivation layer of reactive species on the electrodes, leading to low utilization of the active material as realizing their full capacity is difficult in Li–S batteries. Due to density differences between sulfur (2.03 g cm<sup>-3</sup>) and Li<sub>2</sub>S (1.67 g cm<sup>-3</sup>), almost 80% of extra volume in cathode is necessary to accommodate the precipitated Li<sub>2</sub>S (each mole of sulfur can be transformed into eight moles of Li<sub>2</sub>S).<sup>[6,7]</sup> The morphology of precipitated Li<sub>2</sub>S is rate-dependent, where slower discharge rate leads to lower nuclei density and formation of larger crystallites, while at higher discharge rate more conformal and fine structure. The differences in the morphology may also affect the final volume change. During charging process where Li<sub>2</sub>S is oxidized into soluble polysulfides and at the end of charging, the total volume of the cathode is expected to be lower than at the end of discharging process.<sup>[8]</sup> These issues result in poor cycle life and lithium anode corrosion, low utilization of the active material, poor electronic conductivity, significant volume change, and system efficiency.<sup>[9,10]</sup> (Scheme 1) To make efforts to solve these issues, the most common approach is to physically confine sulfur in various carbon materials. These carbon materials, keep abundant porous structures like porous carbon, carbon fibers, carbon nanotubes (CNTs), carbon spheres, graphene etc., which are prepared via calcination of

Y.-C. Jiang, H. M. U. Arshad, H.-J. Li, S. Liu, Prof. G.-R. Li, Prof. X.-P. Gao  
Institute of New Energy Material Chemistry  
School of Materials Science and Engineering  
Nankai University  
Tianjin 300350, China  
E-mail: guoranli@nankai.edu.cn; xpgao@nankai.edu.cn

 The ORCID identification number(s) for the author(s) of this article can be found under <https://doi.org/10.1002/smll.202005332>.

DOI: 10.1002/smll.202005332



**Scheme 1.** Problems of cathodes in Li-S batteries and progress of host materials.

numerous carbonaceous materials, accompanied with a physical or chemical activation treatment.<sup>[11–16]</sup> Such carbon materials usually adsorb the polysulfide intermediates through high surface area, but usually offer weak interactions toward intermediate polar LiPSs and poor catalytic ability for conversion of polysulfides. That is why some surface chemistry techniques with dopant atoms and functional groups on carbon host materials have been tried to improve performance of sulfur-carbon composite cathodes.<sup>[17–19]</sup>

Beyond carbon materials, metal based polar compounds, such as oxides, sulfides, nitrides, phosphides, and carbides have been investigated as host materials for sulfur cathodes.<sup>[20–29]</sup> In some cases, these inorganic materials improve the cycling performance obviously due to the strong polarity and adsorption to polysulfides. In addition, transition metal oxides as host materials are helpful for obtaining a high volumetric capacity because of high tap density.<sup>[30]</sup>

Single metal oxides, like  $\text{MnO}_2$ ,  $\text{Co}_3\text{O}_4$ , and  $\text{NiO}$ , usually suffer from low electronic conductive ( $\sigma_{e-}$ ) properties and unfavorable stability that limit the performance of energy storage system.<sup>[31–34]</sup> Nanostructures and composite engineering are promising approaches to address issues of single metal oxides.<sup>[35]</sup> Lithium (Li) bond has been well established through polar-polar interactions between intermediate polar LiPSs and lithiophilic surface. Such material design and mechanist understanding are fruitful to explore the unique sulfur host materials which are capable of simultaneously regulating intermediate polar LiPSs crossover and  $\text{Li}_2\text{S}$  deposition. To tune intermediate polar LiPSs transport and regulate  $\text{Li}_2\text{S}$  deposition, integration of multi-metal component in one crystal is highly expected since it potentially combines individual component functions.<sup>[36]</sup> This is the reason that the recent rise of multi-metallic compounds is given more consideration in energy storage system because of their better electronic conductivity( $\sigma_{e-}$ ) and

electrochemical activity performance. For example, spinel cobaltites  $\text{M}_x\text{Co}_{3-x}\text{O}_4$  ( $M = \text{Ni}, \text{Mn}, \text{Zn}, \text{Cu}$ ) and  $\text{FeCo}_2\text{O}_4/\text{CoFe}_2\text{O}_4$  as electrode materials revealed better characteristics for fuel cells, super capacitors, and Li-ion batteries.<sup>[37,38]</sup>

In this review, we focus on the major development of multi-metallic compounds as host materials in cathode for lithium-sulfur batteries, explaining design principles, structure and properties, and electrochemical performances. Finally, some future perspectives and directions are pointed out based on literature, which will further significantly progress in lithium-sulfur batteries.

## 2. Transition Metal Composite Oxides

Transition metal composite oxides involving binary or polynary metal oxides usually show enhanced properties in electricity, optics, and magnetics. According to crystal structure, transition metal composite oxides can be assorted into different types: spinel, perovskite, rock salt, etc. Generally, the transition metal composite oxides have stable structure, relatively high specific surface area, and strong metal-oxygen bonds, as well as electrocatalytic activity of transition metals in some cases, which make the multi-metal compounds preferred materials for sulfur host for improving electrochemical properties.

### 2.1. Spinel

The general formula of spinel-type oxides is  $\text{AB}_2\text{O}_4$ , in which oxygen anions form a face-centered cubic sublattice and two kinds of interstitial sites are available for the cations: tetrahedral and octahedral (**Figure 1a**). Twice as many octahedral sites as tetrahedral sites are occupied by A or B cations. The crystalline phase provides robust structure, small volume change, and various electrochemical properties.<sup>[39]</sup>

#### 2.1.1. $\text{NiCo}_2\text{O}_4$

$\text{NiCo}_2\text{O}_4$  is a mixed valence oxide with spinel structure, where nickel cations occupy the octahedral sites, and cobalt cations distribute over both the octahedral and tetrahedral sites.  $\text{NiCo}_2\text{O}_4$  has intrinsic polarity, which enables its surface metal or oxygen ions synergistically interact with  $\text{S}_x^{2-}$  and  $\text{Li}^+$  ions to immobilize polysulfides and provide electrocatalytic activity.<sup>[40]</sup> Furthermore, the redox couples of  $\text{Co}^{3+}/\text{Co}^{2+}$  and  $\text{Ni}^{3+}/\text{Ni}^{2+}$  coexist in the structure resulting in significant electronic conductivity of spinel  $\text{NiCo}_2\text{O}_4$ , which is superior to those of nickel oxides and cobalt oxides by at least two orders of magnitude.<sup>[41,42]</sup> These properties make  $\text{NiCo}_2\text{O}_4$  a promising host material for sulfur cathode in Li-S batteries.

By nanotechnology,  $\text{NiCo}_2\text{O}_4$  with different structures and morphologies in nanometer scale can be obtained for increasing surface area, stabilizing structure, and shortening diffusion path. Iqbal et al. synthesized hollow microtubes consisting of  $\text{NiCo}_2\text{O}_4$  nanosheets (**Figure 2 a,b**).<sup>[40]</sup> The hollow interior cavity provides structural stability by accommodating volume expansion during cycling process, while outer  $\text{NiCo}_2\text{O}_4$

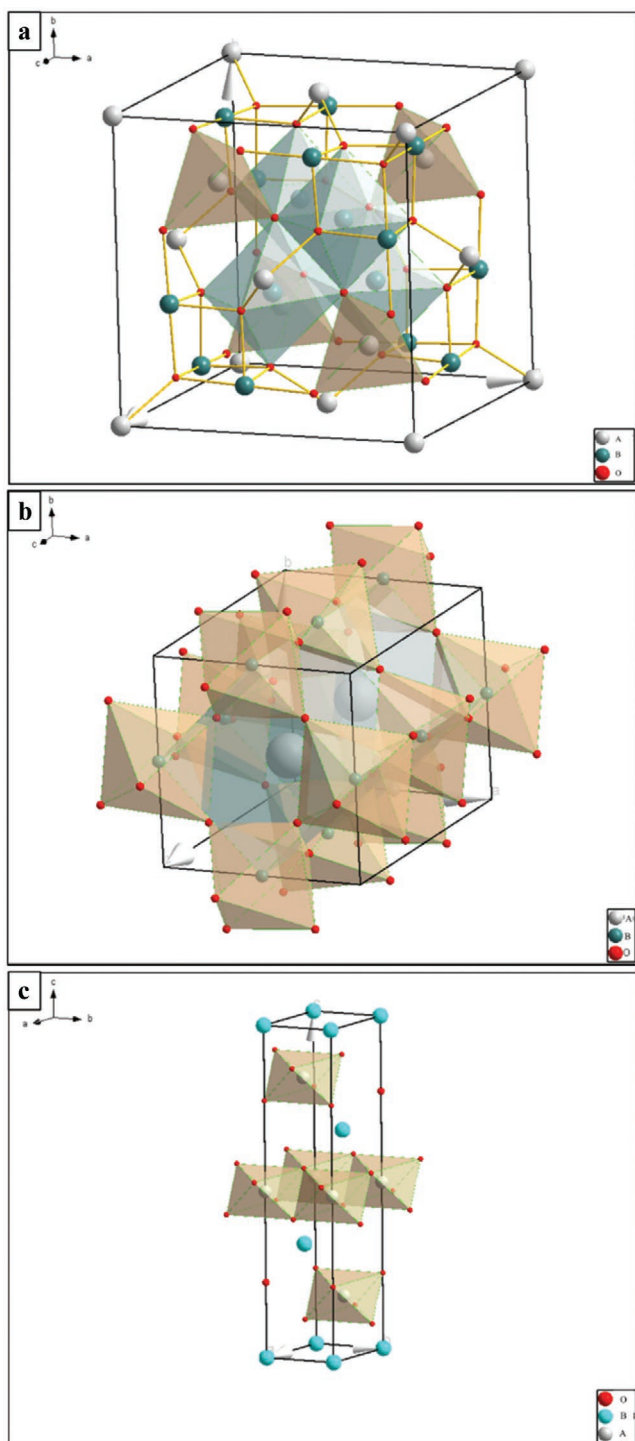


**Figure 1.** The crystal structure of a) spinel, b) perovskite, and c)  $\alpha$ -NaFeO<sub>2</sub> type oxides.

nanosheets not only provide large amount of sulfur encapsulation but also offer a relatively large functional surface for chemically binding of polysulfides. As a cathode material used in lithium–sulfur batteries, the S/NiCo<sub>2</sub>O<sub>4</sub> composite delivers high specific capacity of 1274 mA h g<sup>-1</sup> at 0.2C rate and long cycling performance and a reasonable capacity retention of 66%

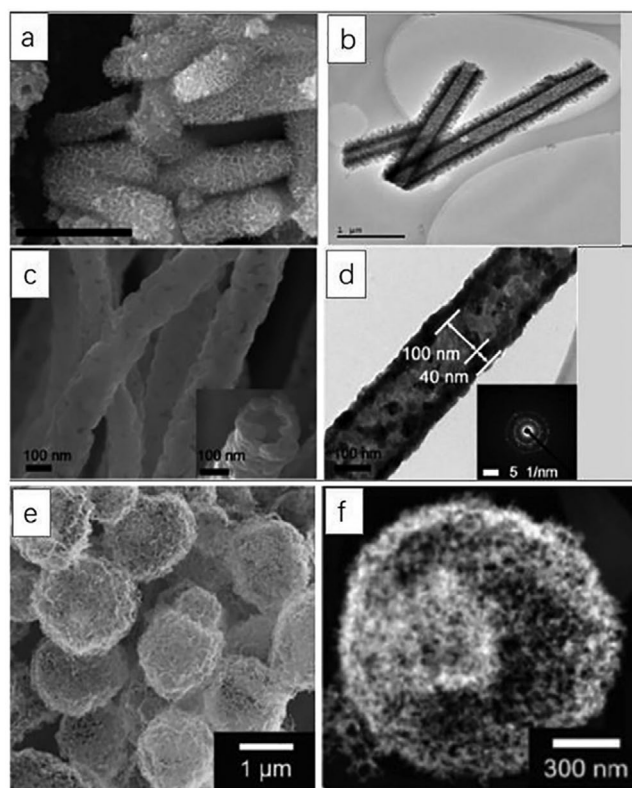


**Figure 2.** The SEM and TEM images of NiCo<sub>2</sub>O<sub>4</sub> as host materials for sulfur cathodes. a,b) NiCo<sub>2</sub>O<sub>4</sub> hollow microtubes. Reproduced with permission.<sup>[40]</sup> Copyright 2017, Elsevier. c,d) NiCo<sub>2</sub>O<sub>4</sub> nanofibers and the corresponding SAED pattern. Reproduced with permission.<sup>[41]</sup> Copyright 2019, Wiley-VCH. e,f) NiCo<sub>2</sub>O<sub>4-x</sub> oxide double-shelled microspheres. Reproduced with permission.<sup>[43]</sup> Copyright 2019, Wiley-VCH.

after 200 cycles at 0.5C rate. However, according to **Table 1**, the sulfur content of the S/NiCo<sub>2</sub>O<sub>4</sub> composite (27%) is much lower than that of the other sulfur composites. Recently, Liu et al. introduced heavy NiCo<sub>2</sub>O<sub>4</sub> nanofibers as carbon-free sulfur immobilizers to fabricate the sulfur-based composites.<sup>[41]</sup> The 1D structure of nanofibers (Figure 2c,d) can provide good conductive networks and ion diffusion paths during dissolution–deposition processes, thus the S/NiCo<sub>2</sub>O<sub>4</sub> composite offers a high gravimetric capacity of 1125 mA h g<sup>-1</sup> at 0.1C rate with low fading rate of 0.039% per cycle over 1500 cycles at 1C rate. Furthermore, due to high tap density (1.66 g cm<sup>-3</sup>), the S/NiCo<sub>2</sub>O<sub>4</sub> composite delivers large volumetric capacity of 1867 mA h cm<sup>-3</sup>, which is almost twice that of the conventional S/carbon composites (850 mA h cm<sup>-3</sup>). As compared with carbon materials, except electrical conductivity, the NiCo<sub>2</sub>O<sub>4</sub> has unique advantages of high density, good adsorption capability, and good electrocatalytic activity.

In order to further enhance the electrical conductivity, Luo et al. introduced abundant oxygen vacancies on octahedral sites of NiCo<sub>2</sub>O<sub>4</sub> by defect engineering.<sup>[43]</sup> The synthesized defective spinel NiCo<sub>2</sub>O<sub>4-x</sub> oxide double-shelled microspheres (NCO-HS) (Figure 2e,f) can homogenize the sulfur distribution as well as buffer the volume variation, which enables high areal capacity (6.3 mA h cm<sup>-2</sup>) and high utilization of sulfur (70 wt%). Hence, as shown in Table 1, the S@NCO-HS composite exhibits

**Table 1.** Summary of studies on NiCo<sub>2</sub>O<sub>4</sub> and its conductive composites as cathode materials for lithium–sulfur batteries.

Materials	Initial capacity [mA h g <sup>-1</sup> ]	Current rate <sup>a)</sup>	Cycle number	Degradation rate per cycle [%]	Sulfur content <sup>b)</sup> [wt%]	Rate performance <sup>c)</sup> at 1C [mA h g <sup>-1</sup> ]	Ref.
NiCo <sub>2</sub> O <sub>4</sub> microtubes	910	0.5C	200	0.170	27	608	[40]
NiCo <sub>2</sub> O <sub>4</sub> nanofibers	872	0.5C	400	0.065	75	≈760 <sup>d)</sup>	[41]
NiCo <sub>2</sub> O <sub>4</sub> microspheres	1221 <sup>d)</sup>	0.2C	800	0.045	70	≈1000 <sup>d)</sup>	[42]
NiCo <sub>2</sub> O <sub>4</sub> nanosheet@CNTs <sup>e)</sup>	961	0.5C	1200	0.038	61.3	783	[44]
NiCo <sub>2</sub> O <sub>4</sub> /porous graphitic carbon	977	0.5C	500	0.062	68.9	727	[45]
NiO-NiCo <sub>2</sub> O <sub>4</sub> @carbon hollow nanocages	1017 <sup>d)</sup>	0.5C	500	0.059	73	821.7	[46]
NiO-NiCo <sub>2</sub> O <sub>4</sub> @PPy hollow polyhedral	963	0.2C	100	0.334 <sup>d)</sup>	61.5	549	[47]

<sup>a)</sup>1C = 1674 mA g<sup>-1</sup>; <sup>b)</sup>Mass percentage of sulfur on the whole cathode; <sup>c)</sup>Capacity of cathode at various C-rate; <sup>d)</sup>Data is estimated from the figure given by paper since authors did not provide the specific value in the reference; <sup>e)</sup>CNTs = carbon nanotubes.

outstanding capacity of 1221 mA h g<sup>-1</sup> with low fading rate of 0.045% per cycle over 800 cycles at 0.2C rate. This proposed strategy based on synergy engineering exposes a novel way to improve electrochemical properties.

Although the electrical conductivity of NiCo<sub>2</sub>O<sub>4</sub> is higher than that of individual Ni and Co oxides, but it is lower than that of carbon materials and conductive polymers. Therefore, some host materials have been developed by combining NiCo<sub>2</sub>O<sub>4</sub> with highly conductive materials in order to enhance the electrical conductivity and structural stability. In this regard, Xiao et al. used 1D CNTs to provide a porous 3D interconnected conductive network and then embed NiCo<sub>2</sub>O<sub>4</sub> nanosheets into CNTs that provide strong binding sites for polysulfide intermediates (Figure 3a).<sup>[44]</sup> With this rational design, the NiCo<sub>2</sub>O<sub>4</sub>@CNT/S composite with sulfur content of 61.3 wt% exhibits specific capacities of 1311 and 575 mA h g<sup>-1</sup> at rates of 0.1C and 2C rate, respectively, and good cycle stability with low capacity fading rate of 0.037% per cycle over 1200 cycles at 0.5C. Moreover, Zhang et al. synthesized a bimetallic-organic-framework-derived nanosulfur host consisting of NiCo<sub>2</sub>O<sub>4</sub> coated with porous graphitic carbon layer, in which the carbon layer acts as a highly conductive matrix for ion transfer.<sup>[45]</sup> With a sulfur content of 68.9%, the cathode

composite delivers a specific capacity of 977 mA h g<sup>-1</sup> at 0.5C rate after 500 cycles.

The NiO-NiCo<sub>2</sub>O<sub>4</sub> heterostructure can facilitate charge transport and enhance the surface reaction kinetics due to the internal electric field (EF). Hu et al. synthesized NiO-NiCo<sub>2</sub>O<sub>4</sub> heterostructure@C hollow nanocage as sulfur host (Figure 3b), which not only provide sufficient space for sulfur loading but also mitigate volumetric variation of sulfur during cycling.<sup>[46]</sup> The as prepared S/NiO-NiCo<sub>2</sub>O<sub>4</sub>@carbon cathode exhibits high specific capacity of ≈1017 mA h g<sup>-1</sup> compared with S/carbon black (690 mA h g<sup>-1</sup>) at 0.5C rate and attains reversible capacity of 716.9 mA h g<sup>-1</sup> with low fading rate of ≈0.059% per cycle after 500 cycles. The outside thin carbon layer can improve the electrical conductivity.

In addition, Xu et al. chose polypyrrole (PPy) as matrix to prepare NiO-NiCo<sub>2</sub>O<sub>4</sub>@PPy hollow polyhedral structure material which is an efficient sulfur immobilizer for Li–S batteries.<sup>[47]</sup> The NiO-NiCo<sub>2</sub>O<sub>4</sub>@PPy is synthesized using the ZIF-67 diamond-shaped polyhedron as a precursor coated with PPy layer on the surface of the hollow NiO-NiCo<sub>2</sub>O<sub>4</sub> via in situ polymerization (Figure 3c). After loading sulfur, the S/NiO-NiCo<sub>2</sub>O<sub>4</sub>@PPy composite exhibits a high initial discharge capacity of 963 mA h g<sup>-1</sup> at 0.2C rate and retained discharge

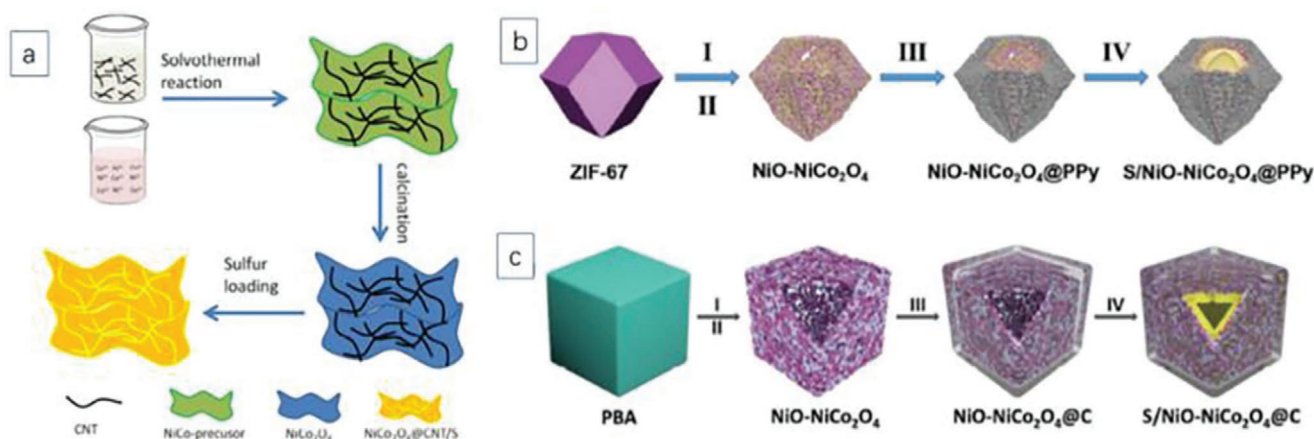


**Figure 3.** The schematic illustrations of the preparation of NiCo<sub>2</sub>O<sub>4</sub>-S nanostructures. a) NiCo<sub>2</sub>O<sub>4</sub>@CNT/S composites. Reproduced with permission.<sup>[44]</sup> Copyright 2017, Wiley-VCH. b) S/NiO-NiCo<sub>2</sub>O<sub>4</sub>@PPy. Reproduced with permission.<sup>[47]</sup> Copyright 2019, The Royal Society of Chemistry. c) S/NiO-NiCo<sub>2</sub>O<sub>4</sub>@C composite. Reproduced with permission.<sup>[46]</sup> Copyright 2018, Wiley-VCH.

capacity of  $641 \text{ mA h g}^{-1}$  after 100 cycles, while the S/NiO-NiCo<sub>2</sub>O<sub>4</sub> cathode without PPy layer shows initial discharge capacity of  $761 \text{ mA h g}^{-1}$  with retained discharge capacity of  $410 \text{ mA h g}^{-1}$  which is lower than that of S/NiO-NiCo<sub>2</sub>O<sub>4</sub>@PPy composite. These results illustrate that the conductive PPy layer significantly increases the electronic conductivity, and the loose structure of PPy is able to alleviate the volume expansion during the charge–discharge process.

From the summarized results in Table 1, it is clear that NiCo<sub>2</sub>O<sub>4</sub> can be competent for hosting sulfur with high loading by designing specific nanostructures and morphologies. Especially in the NiCo<sub>2</sub>O<sub>4-x</sub> double-shelled microspheres, increasing the conductivity via defect engineering make them of higher capacity and better cycle performance. Current research shows that the formation of Li–O bond and metal–sulfur bond is the main way to bind polysulfides in spinel NiCo<sub>2</sub>O<sub>4</sub>, which is accompanied by the reduction of Ni<sup>3+</sup> and Co<sup>3+</sup> ions. All of the (311), (220), and (110) planes of spinel have sufficient binding sites with polysulfides, among which the (311) plane is dominant in all exposed planes, thus it has higher surface energy and is more favorable to absorb LiPS. Besides lithium polysulfides, there are also thiosulfate and polythionate complex formed in reactions by the oxidation of NiCo<sub>2</sub>O<sub>4</sub>, which can be used as mediator to alleviate the shuttle effect. Also, in NiCo<sub>2</sub>O<sub>4</sub>, Ni ions can catalyze the conversion and improve the conductivity of the material in addition to chemically bind polysulfides.

### 2.1.2. NiFe<sub>2</sub>O<sub>4</sub>

The spinel NiFe<sub>2</sub>O<sub>4</sub> is naturally abundant and environmentally friendly, and has same crystalline structure as NiCo<sub>2</sub>O<sub>4</sub>. Although iron oxides usually show disadvantages as electrode materials such as low conductivity and poor lithiation activity, it has been pointed out that the nanostructured NiFe<sub>2</sub>O<sub>4</sub> has the synergistic effects through reinforcement or modification between Ni and Fe to generate the higher electrochemical activity.<sup>[48]</sup> Similar to NiCo<sub>2</sub>O<sub>4</sub>, the NiFe<sub>2</sub>O<sub>4</sub> is a good host material for immobilizing and catalytically transferring the polysulfide, as well as has good plasticity which facilitates the construction of micro-morphology.

Because of the generally lower conductivity of iron oxides, NiFe<sub>2</sub>O<sub>4</sub> is usually combined with carbon materials to improve the conductivity of cathode-based materials. Zhang et al. anchored NiFe<sub>2</sub>O<sub>4</sub> nanoparticles on the carbon nanotubes (CNTs), in which the 3D interwoven structure of CNTs can ensure the uniform dispersion of Ni-Fe oxide nanoparticles and good conduction of electrons.<sup>[49]</sup> (Figure 4a) NiFe<sub>2</sub>O<sub>4</sub> nanoparticles are endowed with sulfiphilic sites to chemically confine polysulfides. The sulfur nanoparticles are well dispersed in the composite, resulting in the high sulfur content (80 wt%) (Figure 5a). As a result, the S/NiFe<sub>2</sub>O<sub>4</sub>-CNTs composite delivers capacities of 1282.7 and  $551.4 \text{ mA h g}^{-1}$  at 0.1C and 5C, respectively, and a stable cyclability with capacity degradation of 0.029% per cycle after 1000 cycles at 1C rate. As for the influence of micro-morphology on the performance of cathode, Fan et al. used NiFe<sub>2</sub>O<sub>4</sub> nanosheets instead of nanoparticles with carbon nanotubes (Figure 4b) which greatly improve the electrochemical properties of the obtained NiFe<sub>2</sub>O<sub>4</sub>/CNTs-S

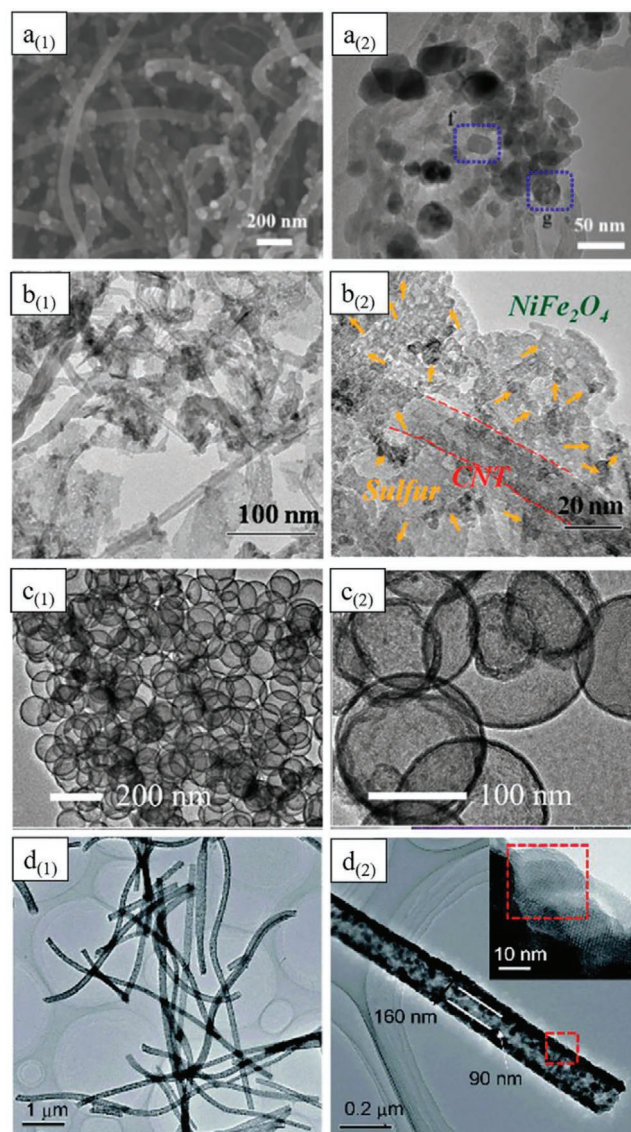


**Figure 4.** SEM and TEM images of NiFe<sub>2</sub>O<sub>4</sub> as host materials for sulfur cathodes. a) NiFe<sub>2</sub>O<sub>4</sub>-CNTs hybrid. Reproduced with permission.<sup>[49]</sup> Copyright 2018, Elsevier. b) Fine S nanoparticles coating CNT/NiFe<sub>2</sub>O<sub>4</sub>. Reproduced with permission.<sup>[50]</sup> Copyright 2015, American Chemical Society. c) NiFe<sub>2</sub>O<sub>4</sub> hollow spheres. Reproduced with permission.<sup>[51]</sup> Copyright 2019, American Chemical Society. d) NiFe<sub>2</sub>O<sub>4</sub> nanofibers. Reproduced with permission.<sup>[52]</sup> Copyright 2018, Springer Nature.

composite (Figure 5b), and show the discharge capacity of 1350 and  $900 \text{ mA h g}^{-1}$  at 0.1C and 1C, respectively with low fading rate of 0.009% after 500 cycles at 1C.<sup>[50]</sup> As shown in Table 2, the material prepared by nanosheet-shaped NiFe<sub>2</sub>O<sub>4</sub> has higher capacity and better cycling performance due to higher efficiency to trap the polysulfide intermediates and stabilizing the cycle performance during charging/discharging process.

Besides, designed morphology of nanostructured NiFe<sub>2</sub>O<sub>4</sub> can improve the adsorption capacity for polysulfides to improve electrochemical performance of cathode. Wang et al. designed a NiFe<sub>2</sub>O<sub>4</sub> hollow spheres (Figure 4c) to bind sulfur physically and absorb the soluble polysulfides chemically.<sup>[51]</sup> NiFe<sub>2</sub>O<sub>4</sub>

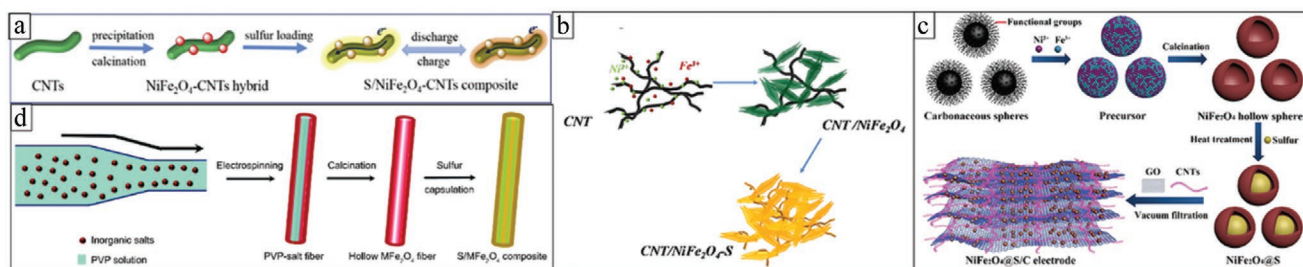


**Figure 5.** The schematic illustrations of the preparation of NiFe<sub>2</sub>O<sub>4</sub>-S nanostructures. a) NiFe<sub>2</sub>O<sub>4</sub>-CNTs hybrid. Reproduced with permission.<sup>[49]</sup> Copyright 2018, Elsevier. b) CNT/NiFe<sub>2</sub>O<sub>4</sub>-S. Reproduced with permission.<sup>[50]</sup> Copyright 2015, American Chemical Society. c) Flexible NiFe<sub>2</sub>O<sub>4</sub>@S/C electrodes. Reproduced with permission.<sup>[51]</sup> Copyright 2019, American Chemical Society. d) NiFe<sub>2</sub>O<sub>4</sub> nanofibers and S/NiFe<sub>2</sub>O<sub>4</sub> composites. Reproduced with permission.<sup>[52]</sup> Copyright 2018, Springer Nature.

hollow spheres are synthesized through an ion adsorption–annealing method, then sulfur is diffused into the NiFe<sub>2</sub>O<sub>4</sub> hollow spheres. Finally, the NiFe<sub>2</sub>O<sub>4</sub>@S composites are introduced into a flexible and conductive skeleton composed of CNTs and reduced graphene oxides (rGO) (Figure 5c). The as-prepared NiFe<sub>2</sub>O<sub>4</sub>@S/rGO–CNT composites as sulfur cathode exhibit high capacity of 1193 mA h g<sup>−1</sup> at 100 mA g<sup>−1</sup> with low fading rate of 0.059% after 500 cycles at 500 mA g<sup>−1</sup>, which is about 1/4 of the S/C electrode under the same condition. This strategy considers as synergism of the physical confinement, polar chemical adsorption, and catalytic conversion, which provides an idea for the preparation of flexible sulfur electrode.

NiFe<sub>2</sub>O<sub>4</sub> nanofibers are prepared and used as host materials by Zhang et al. (Figure 4d).<sup>[52]</sup> In this case, the nanofibers of poly vinylpyrrolidone (PVP) with nickel and iron inorganic salts are prepared by electrospinning and obtain hollow NiFe<sub>2</sub>O<sub>4</sub> fibers after calcination with completely removed PVP template (Figure 5d). The 1D nanostructured S/NiFe<sub>2</sub>O<sub>4</sub> complex is obtained by introducing sulfur with high sulfur content of 82.5 wt%. By comparison as can be seen in Table 2 that the gravimetric capacity of S/NiFe<sub>2</sub>O<sub>4</sub> composite at 0.1C rate is 963.6 mA h g<sup>−1</sup> with fading rate of 0.152% per cycle, which is much higher than others. With high tap density, the S/NiFe<sub>2</sub>O<sub>4</sub> composites show high volumetric capacity of 1281.7 mA h cm<sup>−3</sup> at 0.1C rate.

Similar to NiCo<sub>2</sub>O<sub>4</sub>, NiFe<sub>2</sub>O<sub>4</sub> also binds LiPs mainly through the (311) plane, in which the absorption energy of Li<sub>2</sub>S<sub>8</sub> is 1.23 eV. Li–O bonds are formed when NiFe<sub>2</sub>O<sub>4</sub> binds LiPs with high Li/S ratio, but S–O bonds are formed when NiFe<sub>2</sub>O<sub>4</sub> binds LiPs with low Li/S ratio, which is slightly different from NiCo<sub>2</sub>O<sub>4</sub>. And the interface charge transfer resistance (*R*<sub>ct</sub>) and Warburg impedance (*W*<sub>0</sub>) are slightly larger than

NiCo<sub>2</sub>O<sub>4</sub>, making it slightly lower in initial capacity. Moreover, in NiFe<sub>2</sub>O<sub>4</sub>, Ni ions mainly play the role of binding polysulfide and electrocatalysis.

### 2.1.3. ZnCo<sub>2</sub>O<sub>4</sub>

Unlike the spinel NiCo<sub>2</sub>O<sub>4</sub> where octahedral sites are occupied by both Ni<sup>3+</sup> and Co<sup>3+</sup>, in spinel ZnCo<sub>2</sub>O<sub>4</sub>, Zn<sup>2+</sup> only occupies tetrahedral sites, while octahedral sites are fully occupied by Co<sup>3+</sup>, so ZnCo<sub>2</sub>O<sub>4</sub> has a regular structure and Zn<sup>2+</sup> has an invariable oxidation state.<sup>[53]</sup> Although ZnCo<sub>2</sub>O<sub>4</sub> is isomorphic to the Co<sub>3</sub>O<sub>4</sub> crystal structure, the substitution of Co<sup>2+</sup> by Zn<sup>2+</sup> makes it cheaper and more environmentally friendly. In addition, ZnCo<sub>2</sub>O<sub>4</sub> has narrow energy bandgap and low valence/conduction band.<sup>[54]</sup> Because of these unique properties, ZnCo<sub>2</sub>O<sub>4</sub> and its modifications are widely used in lithium-ion battery, supercapacitors, catalysts, and other fields.<sup>[55–58]</sup>

Similar to Co<sub>3</sub>O<sub>4</sub>, the ZnCo<sub>2</sub>O<sub>4</sub> is not as conductive like NiCo<sub>2</sub>O<sub>4</sub>, so it also needs to be combined with other conductive materials to make composites and used as electrode material. Sun et al. prepared ZnCo<sub>2</sub>O<sub>4</sub>@N-RGO composite as sulfur host material with sulfur content up to 82%.<sup>[59]</sup> (Figure 6) They fabricate a N-doped graphene oxide (N-RGO) which serves as conductive network and steady scaffold and then integrates ZnCo<sub>2</sub>O<sub>4</sub> with N-RGO. The N-RGO sheets not only exhibit a large surface area, which ensures uniform distribution of ZnCo<sub>2</sub>O<sub>4</sub> nanotube and high sulfur loading, but also present a large interface with active sites with ZnCo<sub>2</sub>O<sub>4</sub> to effectively binding sulfur and polysulfides by forming polar N–Li and Zn/Co–S bonds. The ZnCo<sub>2</sub>O<sub>4</sub>/N-RGO composite exhibits a discharge capacity of 1061 mA h g<sup>−1</sup> at 800 mA g<sup>−1</sup> with high initial coulombic efficiency of almost 100%.

**Table 2.** Summary of studies on NiFe<sub>2</sub>O<sub>4</sub> and its conductive composites as cathode materials for lithium–sulfur batteries.

Materials	Initial capacity [mA h g <sup>−1</sup> ]	Current rate <sup>a)</sup>	Cycle number	Degradation rate per cycle [%]	Sulfur content <sup>b)</sup> [wt%]	Rate performance <sup>c)</sup> at 1C [mA h g <sup>−1</sup> ]	Ref.
NiFe <sub>2</sub> O <sub>4</sub> nanoparticles/CNTs <sup>e)</sup>	1282.7	0.1C	1000	0.029	80	824	[49]
NiFe <sub>2</sub> O <sub>4</sub> nanosheet/CNTs <sup>e)</sup>	1350	0.1C	500	0.009	76	900	[50]
NiFe <sub>2</sub> O <sub>4</sub> hollow spheres/CNTs <sup>e)</sup> -rGO <sup>f)</sup>	1193 <sup>d)</sup>	0.06C	500	0.059 <sup>d)</sup>	70	703(at 1.2C) <sup>d)</sup>	[51]
NiFe <sub>2</sub> O <sub>4</sub> nanofibers	963.6	0.1C	200	0.152	82.5	625.9	[52]

<sup>a)</sup>1C = 1674 mA g<sup>−1</sup>; <sup>b)</sup>Mass percentage of sulfur on the whole cathode; <sup>c)</sup>Capacity of cathode at various C-rate; <sup>d)</sup>Data is estimated from the figure given by paper since authors did not provide the specific value in the reference; <sup>e)</sup>CNTs = carbon nanotubes; <sup>f)</sup>rGO = reduced graphene oxides.

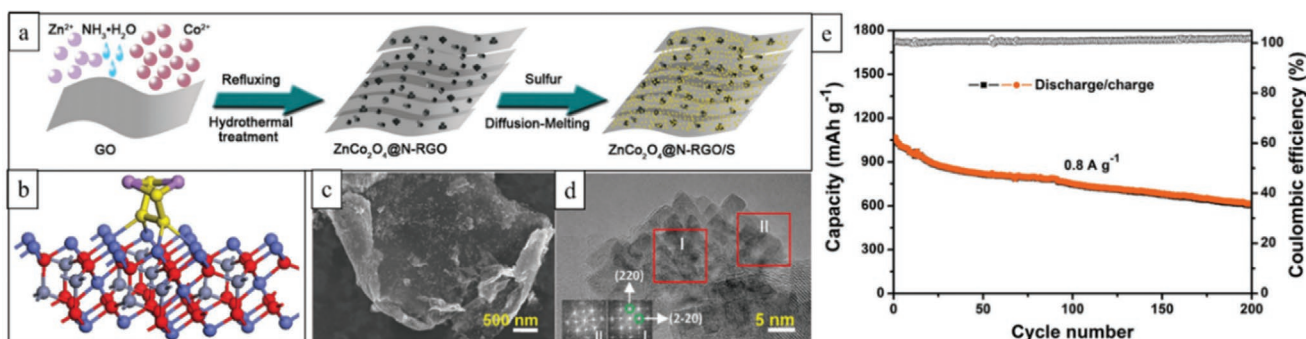


**Figure 6.** Morphology, structure, and electrochemical evaluation of the ZnCo<sub>2</sub>O<sub>4</sub>@N-RGO(l) hybrid. a) Schematic illustration of the synthesis of ZnCo<sub>2</sub>O<sub>4</sub>@N-RGO and ZnCo<sub>2</sub>O<sub>4</sub>@N-RGO/S. b) The optimized atomic geometries of Li<sub>2</sub>S<sub>4</sub> adsorbed on ZnCo<sub>2</sub>O<sub>4</sub> (111) crystal plane. Sulfur: yellow, lithium: purple, Zn/Co: blue and grey, oxygen: red. c, d) FESEM and HRTEM image of the ZnCo<sub>2</sub>O<sub>4</sub>@N-RGO(l) hybrid showing the distinguishable microstructures. e) Cycling performance at a current density of 0.8 A g<sup>-1</sup>. Reproduced with permission.<sup>[59]</sup> Copyright 2018, Wiley-VCH.

After 200 cycles, the capacity remains at 614 mA h g<sup>-1</sup> with fading rate of 0.210% per cycle. In general, the properties of ZnCo<sub>2</sub>O<sub>4</sub> are very similar to that of Co<sub>3</sub>O<sub>4</sub> and as a sulfur host material, the ZnCo<sub>2</sub>O<sub>4</sub> mainly reduces the shuttle effect by forming chemical bond with polysulfide. Besides, the ZnCo<sub>2</sub>O<sub>4</sub> has cost effectiveness and less toxicity as Zn<sup>2+</sup> replaced Co<sup>2+</sup>, as well as the better stability due to spinel structure.

Different from the former two materials, the spinel ZnCo<sub>2</sub>O<sub>4</sub> mainly binds LiPs on the (111) plane with a binding energy of -3.1 eV. The main bonds formed are Zn-S bonds and Co-S bonds, which effectively bind polysulfide in the cathode. Moreover, the discharge voltage of Li-S battery with ZnCo<sub>2</sub>O<sub>4</sub> as sulfur host is slightly lower than that of the other two materials, implying more severe polarization caused by the sluggish kinetics of ions.

## 2.2. Perovskite

The general formula of perovskite oxides can be expressed as ABO<sub>3</sub>, where A is a rare-earth or alkaline-earth cation coordinating with 12 oxygen ions and B is a transition-metal cation coordinating with six oxygen ions. In the perfect perovskite, A cations and O anions form a cubic packing, and B cations are filled with octahedral sites of the body center.<sup>[60]</sup> (Figure 1b) The skeleton connected by oxygen octahedral with common vertex has large voids that allow it to maintain structural stability even if it produces a large number of defects or is filled with other types of cations. However, the crystal structure may be distorted to tetragonal, orthorhombic, or rhombohedral structure because of the variation or substitution of A and/or B cations with different sizes and valences.<sup>[61]</sup> The partial replacement of cations at A and/or B sites with other metal ions can greatly change the properties of perovskite oxides, such as conductivity or catalytic activity, so that it can better adapt to the requirements of different host materials while retaining the original structural properties.

### 2.2.1. BaTiO<sub>3</sub>

BaTiO<sub>3</sub> is one of the most widely used ferroelectric materials, which can induce “spontaneous polarization” due to

its asymmetric crystal structure under suitable conditions. The “spontaneous polarization” causes internal electric field and induces macroscopic charges on the surface of ferroelectrics, which chemically adsorb the outside polar molecules to screen these charges.<sup>[62,63]</sup> Therefore, the use of BaTiO<sub>3</sub> as an additive or host material for Li-S batteries can enhance the entrapment of polar polysulfides and improve the stability of Li-S batteries. Xie et al. first added BaTiO<sub>3</sub> as an additive to the cathode materials.<sup>[64]</sup> By adding 10 wt% of BaTiO<sub>3</sub> nanoparticles, the Li-S cell with S/C electrodes exhibits an initial capacity of 1143 mA h g<sup>-1</sup> at 0.2C rate and maintains a reversible discharge capacity of 835 mA h g<sup>-1</sup> after 100 cycles. In contrast, the cell without any additive exhibits similar initial capacity at 0.2C rate but retains discharge capacity is only 407 mA h g<sup>-1</sup> after 100 cycles, which is less than half that of with addition of additive. This indicates that the polysulfides can be anchored by adding BaTiO<sub>3</sub> nanoparticles into cathode material, which effectively improves the rate and cycle performance of Li-S batteries. In order to enhance the binding capacity of internal electric field, Wang et al. combined TiO<sub>2</sub> and BaTiO<sub>3</sub> into coherent nanosized junctions using for sulfur host materials for Li-S batteries.<sup>[65]</sup> The obtained porous TiO<sub>2</sub>/BaTiO<sub>3</sub> heterostructure not only binds the polysulfide, but also creates an internal electric field at the interface due to the misaligned energy levels of the conduction and valence bands of TiO<sub>2</sub> and BaTiO<sub>3</sub>, which enhances the electron's transportation and charge separation at the junction interface. After sulfur loading, the TiO<sub>2</sub>/BaTiO<sub>3</sub>-S composite demonstrates high initial capacity of 898 mA h g<sup>-1</sup> which decreases to 541 mA h g<sup>-1</sup> after 500 cycles with a capacity retention rate of 60% and low fading rate of 0.08% per cycle, showing better capacity and cycle performance of TiO<sub>2</sub>/BaTiO<sub>3</sub>-S than that of BaTiO<sub>3</sub>-S. It is proved that the internal electric field created by TiO<sub>2</sub>/BaTiO<sub>3</sub> heterostructure can suppress the shuttle effect, increasing the Li<sup>+</sup>/electron transportation and the separation at their interface, which can efficiently improve the conversion kinetics of polysulfides and rate performance.

The hybridization between titanium 3d states and oxygen 2p states gave BaTiO<sub>3</sub> the property of “spontaneous polarization,” which creates an internal electric field within the particles that can absorb polar polysulfides.<sup>[66]</sup> This offers a new polysulfide trapping strategy to suppress the polysulfide shuttle effect. Moreover, this kind of “spontaneous polarization” of

ferroelectricity exists not only in BaTiO<sub>3</sub>, but also in many other perovskite oxides, so there is still a lot of room for exploration in the future.

### 2.2.2. Lanthanum Strontium Oxides

Lanthanum strontium oxides are a class of perovskite-type heavy metal oxides with electrocatalytic properties, which means that they usually have high mass density. To increase the conductivity, Hao et al. proposed a novel perovskite La<sub>0.6</sub>Sr<sub>0.4</sub>CoO<sub>3-δ</sub> nanofibers which is composed of interlinked nanoparticles, and then coat it with CNTs.<sup>[67]</sup> La<sub>0.6</sub>Sr<sub>0.4</sub>CoO<sub>3-δ</sub> (LSC) is the most conductive material of La<sub>1-x</sub>Sr<sub>x</sub>CoO<sub>3-δ</sub> (x = 0–1) family. La<sub>0.6</sub>Sr<sub>0.4</sub>CoO<sub>3-δ</sub> not only exhibits strong immobilization capability for polysulfides via Co–S bonds but also facilitates the electrochemical redox process of the insulating S through the high conductivity provided by oxygen vacancies. The cell composed of electrospun of La<sub>0.6</sub>Sr<sub>0.4</sub>CoO<sub>3-δ</sub> nanofibers-CNTs composites delivers an average capacity of 996 mA h g<sup>-1</sup> at 0.5C rate with low fading rate of 0.039% per cycle over 400 cycles. The 1D structure of La<sub>0.6</sub>Sr<sub>0.4</sub>CoO<sub>3-δ</sub> nanofibers not only have interconnected conductive channels that promise high-efficiency electron and ion transfer, but also can stabilize the electrode structure and therefore improve the cycling stability with high sulfur content (5.4 mg cm<sup>-2</sup>). This work provides a good starting point to use the chemically stable perovskite oxides with tunable component as sulfur host materials. More recently, Liu et al. prepared 1D nanofibers with a high theoretical density of La<sub>0.8</sub>Sr<sub>0.2</sub>MnO<sub>3</sub> by electrospinning. Benefitting from its high density (1.69 mg cm<sup>-2</sup>), the S/ La<sub>0.8</sub>Sr<sub>0.2</sub>MnO<sub>3</sub> composite shows an extremely high volumetric energy density of 2727 Wh L<sup>-1</sup>.<sub>cathode</sub> with a high sulfur loading of 6.2 mg cm<sup>-2</sup>, which is more than twice that of S/carbon cathode. Moreover, as La<sub>0.8</sub>Sr<sub>0.2</sub>MnO<sub>3</sub> is electrochemically stable in the Li–S battery operation window, the S/ La<sub>0.8</sub>Sr<sub>0.2</sub>MnO<sub>3</sub> composite exhibits a relatively good capacity of 792 mA h g<sup>-1</sup> and cycle stability of 0.21% degradation per cycle at 0.1C. This research is an effective attempt at high energy density Li–S batteries.<sup>[68]</sup>

The transition metal ions in the lanthanum strontium oxide can adsorb polysulfides through the change of valence state, which is usually concentrated on the (110) plane. And Sr doping can enhance the adsorption energy of transition metal ions through valence variation along with oxygen vacancy, thus enhancing its absorption of polysulfides.

### 2.2.3. Complex Perovskite Oxides

Complex perovskite oxides are generally doped with a variety of cations, hence the general structure is changed to A<sub>x</sub>A'<sub>1-x</sub>B<sub>y</sub>B'<sub>1-y</sub>O<sub>3-δ</sub>.<sup>[61]</sup> The metal cations in the perovskite nanoparticles (PrNPs) with complex composition can be combined, reduced and re-oxidized without any limitation, thus producing a large number of active sites and oxygen vacancies, which is favorable for the entrapment of polysulfide. Therefore, adding PrNPs into conductive carbon materials can effectively bind polysulfide and reduce the shuttle effect. Kong et al. prepared a kind of Ba<sub>0.5</sub>Sr<sub>0.5</sub>Co<sub>0.8</sub>Fe<sub>0.2</sub>O<sub>3-δ</sub> perovskite nanoparticles as

promoters to immobilize the polysulfide and guide Li<sub>2</sub>S deposition.<sup>[36]</sup> These nanoparticles contain large numbers of binding sites (Sr) and oxygen vacancies that promote the surface interactions of polysulfides and PrNPs, as well as variable and high valence transition metal ions (Fe and Co ions) that capable to further benefit the LiPSs regulation. Cell with 10 wt% PrNPs exhibits an initial capacity of 793 mA h g<sup>-1</sup> at 0.5C rate which decreases to 695 mA h g<sup>-1</sup> after 200 cycles with fading rate of 0.062% per cycle. In contrast, cell without PrNPs (CNTs/S electrode) exhibits an initial capacity of 835 mA h g<sup>-1</sup> at 0.5C rate, but after 200 cycles the capacity decreases to 437 mA h g<sup>-1</sup> with fading rate of 0.23% per cycle, which is about four times that of the cell containing PrNPs. The resulting carbon material with PrNPs presents a plenty of electron-conductive and LiPSs adsorptive interfaces to promote the nucleation and growth of Li<sub>2</sub>S, which results more Li<sub>2</sub>S deposits in the electrode discharge profiles and leads to improve the cycle performance. In order to enhance the polysulfides entrapment, Chen et al. added flower-like MoS<sub>2</sub>, BaMn<sub>0.9</sub>Mg<sub>0.1</sub>O<sub>3</sub> perovskite nanoparticles and CNTs layers on the carbon cloth (DCC).<sup>[69]</sup> The MoS<sub>2</sub> can endow ample polar active sites to suppress polysulfide shuttle effect and achieve long-term cycle stability. However, since a single polar host like MoS<sub>2</sub> cannot meet the high sulfur loading requirements owing to the limited number of absorption sites, BaMn<sub>0.9</sub>Mg<sub>0.1</sub>O<sub>3</sub> perovskite nanoparticles need to be crosslinked to MoS<sub>2</sub> layer to overcome this shortcoming. Subsequently, the conductivity and flexibility of the composites are enhanced by the CNTs layer. With excellent binding ability and ultrahigh sulfur loading of 5.2 mg cm<sup>-2</sup>, the DCC@MoS<sub>2</sub>/PNP/CNTs/S composite delivers a discharge capacity of 871 mA h g<sup>-1</sup> at 1C with low fading rate (0.02%) per cycle over 800 cycles.

In complex perovskite particles, A ions are usually heavy Ba or Sr ions, which endow PrNPs with the larger tap density to increase its volume energy density, and the B ions are usually variable- and high-valence transition metal ions to absorb polysulfides and catalyze its conversion. Therefore, PrNPs can effectively promote the conversion of LiPs and improve the electrochemical properties of cathode through the synergistic effect of these two kinds of ions.

### 2.3. NaFeO<sub>2</sub>-Type Oxides

The NaFeO<sub>2</sub>-type oxides have a general formula of ABO<sub>2</sub>, where A(I) is alkali cations and B(III) is transition-metal cations. There are two common structures of NaFeO<sub>2</sub>-type oxides, α-NaFeO<sub>2</sub>-type and β-NaFeO<sub>2</sub>-type. The monovalent and trivalent cations of α-NaFeO<sub>2</sub>-type oxides occupy the octahedral position in the dense cubic packing of oxygen-anion, and are ordered along the [111] direction of the rock salt lattice, resulting in a 2D layered structure.<sup>[70]</sup> (Figure 1c) As for β-NaFeO<sub>2</sub>-type oxides, monovalent and trivalent cations regularly occupy the divalent cation site, and all cations are in fourfold and tetrahedral coordination to oxygen atoms.<sup>[71]</sup> α-NaFeO<sub>2</sub>-type oxides are widely used in lithium-ion battery because of their stable framework and structure that allow the ions to move between layers, which lead to structural stability and better electrochemical performance while the β-NaFeO<sub>2</sub>-type oxides have become a potential semiconductor material because of their bandgaps with a wide range of energies.<sup>[71,72]</sup>

LiCoO<sub>2</sub> is one of the most widely used  $\alpha$ -NaFeO<sub>2</sub>-type material, which has high operating voltage and stable cycle performance due to its favorable 2D plane structure through which lithiation and delithiation can occur.<sup>[73]</sup> However, it also has some shortcomings like high cost and poor stability. By doping with other metal cations, the capacity, rate capability, and operating voltage of  $\alpha$ -NaFeO<sub>2</sub> can be increased effectively and the cost can be reduced. Currently, the most commonly used mixed-cations composites, such as LiNi<sub>x</sub>Co<sub>y</sub>Mn<sub>1-x-y</sub>O<sub>2</sub> (NCM) and LiNi<sub>x</sub>Co<sub>y</sub>Al<sub>1-x-y</sub>O<sub>2</sub> (NCA), can improve the performance of the electrode by overlithiation. Due to high tap density of commercial NCM, Wang et al. combined LiNi<sub>0.8</sub>Co<sub>0.1</sub>Mn<sub>0.1</sub>O<sub>2</sub> (NCM811) microspheres with sulfur to prepare a carbon-free sulfur cathode of Li-S batteries.<sup>[74]</sup> The structure of the microspheres establishes stable conductive frameworks and porous channels to facilitate the electron transfer and effective ions diffusion. The composition of Ni, Co, and Mn in NCM not only has been proved to be sulphophilic, which can reduce the shuttle effect by bonding with polysulfide, but also promotes the conversion of polysulfide because of high electrochemical catalytic ability. With this carbon-free S/NCM811 composite, cell cycled over 500 times showed a low decay rate of 0.057% per cycle at 0.1C rate. In addition, the relatively low exposed surface area and moderately stacked porosity by high tap density result in a large volumetric capacity of 1601.9 mA h cm<sup>-3</sup>, which is 2.3 times higher than that of S/carbon composites. Shi et al. used LiNi<sub>0.8</sub>Co<sub>0.15</sub>Al<sub>0.05</sub>O<sub>2</sub> (NCA) powder formed with sulfur for electrode as trapper and accelerator of polysulfides.<sup>[75]</sup> The electronic conductivity and Li<sup>+</sup> diffusion coefficient ( $D_{Li^+}$ ) of the electrode with S/NCA composite in Li-S batteries are significantly improved. The active sites and variable-valence of Ni and Co promote the transfer of ions and enhance the redox activity of LiPSs, resulting in excellent cycling and rate performance as well as low self-discharge behavior. S/NCA composite exhibits a high discharge capacity of 755.4 mA h g<sup>-1</sup> at 1C rate and a low capacity fading rate of 0.02% per cycle over 500 cycles. The usage of NaFeO<sub>2</sub>-type oxides provides a convenient and effective strategy for enhancing the electrochemical performance of Li-S battery.

NCM and NCA have a similar mechanism of interaction with polysulfides. The adsorption of polysulfides mainly occurs on (104), (003) and (110) planes, where (104), (003) planes mainly form Li-O bond and (104), (110) planes mainly form Co-S bond. The (110) planes have the largest adsorption energy to polysulfides. With the increase in Ni content, the amount of Ni<sup>3+</sup> ions increases gradually, which is a bifunctional carrier with adsorption and catalytic functions, so the electrochemical performance of cathode is gradually improved. The layered structure of  $\alpha$ -NaFeO<sub>2</sub>-type material can keep the stability in the layer while transferring and diffusing ions between the layers, which allows it to be a strong host as well as a good conductor. It is a potential material for preparing cathode without adding conductive carbon material.

## 2.4. Ion-Substituted Metal Oxides

The substitution of ions in single oxides can maintain the stability of the crystal while destroying the short-range structure of crystal, resulting in more defects and oxygen vacancies, which

improve the internal conductivity of the material. Because of variable valence and large ionic radius of transition metal cations, the electrical conductivity and electrocatalytic activity of the ion-substituted oxides are increased correspondingly, thereby enhancing their electrochemical properties. Due to their hydrophilic nature and presence of hydroxyl groups on surface, MgO nanoparticles are capable to absorb polysulfides. Furthermore, Mg as alkaline earth metal, has higher electropositivity than other transition metals such as Mn and Ni, so Mg oxides can be used as additives to improve the capacity and cycle stability of Li-S batteries.<sup>[76]</sup> Replacing Mg cations with other transition metal cations, the MgO structure improves not only its conductivity but also electrochemical catalytic ability.<sup>[72]</sup> Therefore, the ion-substituted magnesium oxide is an ideal additive to improve electrochemical performance of Li-S batteries.

### 2.4.1. Mg<sub>0.6</sub>Ni<sub>0.4</sub>O

Mg<sub>0.6</sub>Ni<sub>0.4</sub>O is one of the earliest oxides proposed as an additive for Li-S batteries. Early in 2004, Ahn and co-workers increase the initial capacity of Li-S batteries by adding Mg<sub>0.6</sub>Ni<sub>0.4</sub>O (15 wt%) nanoparticles (30–50 nm) to sulfur based cathode.<sup>[77]</sup> The nano-sized Mg<sub>0.6</sub>Ni<sub>0.4</sub>O has the same crystal structure like MgO, which means it can absorb polysulfide and keep liquid electrolyte like MgO, while the substitution of Ni cation gives catalysis of dissociating chemical bond. The initial capacity is increased from 741 mA h g<sup>-1</sup> (without additives) to 1185 mA h g<sup>-1</sup> (more than 60%), by improving rate capability as well as porosity of the sulfur electrode, which means that the addition of Mg<sub>0.6</sub>Ni<sub>0.4</sub>O can effectively prevent the polysulfide to mix with electrolyte that reduce the shuttle effect. Although the electrochemical performance has been improved, the capacity decreased to  $\approx$ 1000 mA h g<sup>-1</sup> after 50 cycles which indicate poor cycle durability and polysulfide retention of the cathode. Subsequently, Tang et al. used Mg<sub>0.6</sub>Ni<sub>0.4</sub>O hollow nanofibers (100–200 nm in diameter) as additives to improve the electrochemical properties of Li-S batteries, due to 1D structure of nanofibers, larger surface area, and excellent pore connectivity.<sup>[78]</sup> Sulfur is mixed with Mg<sub>0.6</sub>Ni<sub>0.4</sub>O nanofibers to form composites and calcines at different temperatures. The results show that the calcined Mg<sub>0.6</sub>Ni<sub>0.4</sub>O at 700 °C improves the initial capacity from 595 to 910 mA h g<sup>-1</sup> but keeps reversible capacity of 554 mA h g<sup>-1</sup> after 20 cycles, exhibiting that there is no significant improvement in cycle stability. To solve this problem, Zhang et al. added Mg<sub>0.6</sub>Ni<sub>0.4</sub>O nanoparticles (20–50 nm) to the S/polyacrylonitrile (PAN) due to its high sulfur utilization and excellent initial capacity.<sup>[79]</sup> The S/PAN/Mg<sub>0.6</sub>Ni<sub>0.4</sub>O composite as cathode material not only delivers a higher initial capacity of 1223 mA h g<sup>-1</sup> at 0.1C rate, but also maintains around 100% capacity after the first 100 cycles, greatly improving the cycle durability as compared with other works. Despite of its high polysulfide retention, the low sulfur content (32 wt%) of this composite still needs to be improved.

### 2.4.2. Mg<sub>0.8</sub>Cu<sub>0.2</sub>O

Cu<sup>2+</sup> cation has nearly the same radius as Mg<sup>2+</sup> cation but better conductivity. Therefore the substitution of Cu<sup>2+</sup> cation

with MgO not only keeps the structure stability but also gains higher conductivity.<sup>[80]</sup> Zhang et al. used nanosized Mg<sub>0.8</sub>Cu<sub>0.2</sub>O for S/crystalline vanadium pentoxide (c-V<sub>2</sub>O<sub>5</sub>) cathode to restrain the dissolution and aggregation of the polymer and sulfur.<sup>[81]</sup> The cathode, containing 10 wt% additive and 38 wt% sulfur, exhibits an initial capacity of 545 mA h g<sup>-1</sup> and a capacity retention rate of 77.5% (422 mA h g<sup>-1</sup>) after 30 cycles, while the S/c-V<sub>2</sub>O<sub>5</sub> cathode without additive shows the initial capacity of 400 mA h g<sup>-1</sup> and maintains at 227 mA h g<sup>-1</sup> after 30 cycles. The results show that the addition of Mg<sub>0.8</sub>Cu<sub>0.2</sub>O powder can improve the rate performance and cycle stability of the cathode. However, the effect of crystalline vanadium pentoxide used as sulfur host is not clear in this study.

The adsorption of ion-substituted MgO mainly takes place on (111), (200), and (222) planes, where Mg<sup>2+</sup> mainly plays the role of adsorbing electrolyte and catalyzing the dissociation of S–S single bonds, and the substituted transition metal ions can combine with polar polysulfides to reduce the shuttle effect. Using ion-substituted MgO as an additive can effectively reduce the interface R<sub>ct</sub> of cathode and shorten the voltage gap of redox potential, thus reducing the polarization and enhancing kinetics.

### 3. Multi-Metal Chalcogenides

S, Se, and O are all members of VIA group, so the physical and chemical properties of metal sulfides and selenides are similar to those of oxides. However, the metal M–S and M–Se bonds are weaker than the M–O bonds, therefore metal sulfides and selenides have higher kinetic reactivity and better rate capability than corresponding oxides.<sup>[82]</sup> Excellent skeleton flexibility gives sulfides and selenides various nanostructure, but generally poor conductivity also limits their further application. Therefore, most of the current research has designed them with special nanostructures or combined them with carbon materials.

#### 3.1. Sulfides

Recently, with the development of various synthetic methods, the metal sulfides have been applied as sulfur host materials of Li–S batteries. Metal sulfides have strong affinity to sulfur-containing species, and their low lithiation voltage can avoid overlap in the working voltage window of Li–S batteries.<sup>[83]</sup> In addition, metal sulfides have more metallic phases and better structural flexibility than oxides, which can be designed as more complex and fine microstructures. Due to special structures of nanosized transition metal sulfides with excellent conductivity, polysulfide absorption, and electrocatalytic activity, they are considered as potential candidates for Li–S battery.

##### 3.1.1. NiCo<sub>2</sub>S<sub>4</sub>

The transition metal sulfides used as host materials are usually mono-metal sulfides. Common ones are CoS<sub>2</sub> and NiS<sub>2</sub> due to strong reaction with polysulfide and facilitate the redox kinetics, which can improve the conductivity of the electrode.<sup>[84]</sup>

By combining two materials, bimetal sulfide NiCo<sub>2</sub>S<sub>4</sub> is used as a sulfur host to bind the polysulfides and reduces the shuttle effect. Because of the large volume change and excellent flexibility of NiCo<sub>2</sub>S<sub>4</sub>, complex secondary microstructures are usually designed as nanoscale electrochemical reaction vessels to immobilize and catalyze the LiPSs.

Tan et al. firstly designed the hollow NiCo<sub>2</sub>S<sub>4</sub> sphere with an egg yolk–shell (Figure 7a) that can both load sulfur and mitigate volumetric variation of sulfur during cycling via facile anion exchange method (Figure 8a).<sup>[85]</sup> The S/NiCo<sub>2</sub>S<sub>4</sub> composite with 70 wt% sulfur maintains a capacity of 318.9 mA h g<sup>-1</sup> at 0.5C rate with fading rate of 0.074% per cycle after 500 cycles. In the same year, Wu et al. synthesized NiCo<sub>2</sub>S<sub>4</sub> with a distinctive urchin-like structure.<sup>[86]</sup> The spikes of the urchin-like structure with a diameter of about 100 nm are composed of dotted porous primary particles (Figure 7b), which can load large amounts of sulfur while leaving space for volume changes (Figure 8b). The NiCo<sub>2</sub>S<sub>4</sub>/S composite loaded with sulfur (sulfur content = 48.5 wt%) provides an initial capacity of 1028 mA h g<sup>-1</sup> at 0.1C rate and decreases to 421 mA h g<sup>-1</sup> after 100 cycles, which shows a poor cycle stability. To improve cycle stability, Dai et al. constructed a 2D Chinese knots-like network with 1D nanostructured NiCo<sub>2</sub>S<sub>4</sub> nanotubes (Figure 7c).<sup>[87]</sup> The internal connectivity of the special hollow structure not only accommodates the volumetric expansion of sulfur, but also provides structural encapsulation for polysulfide (Figure 8c). The hollow structure of the NiCo<sub>2</sub>S<sub>4</sub> nanotube with high sulfur content of 71 wt% exhibits a high capacity of 932 mA h g<sup>-1</sup> at 1C rate with a low fading rate of 0.02% per cycle over 1000 cycles, which significantly improves the cycle performance of S/NiCo<sub>2</sub>S<sub>4</sub> composites. Another attempt recently proposed by Li et al. was using self-assembled NiCo<sub>2</sub>S<sub>4</sub> granule with secondary open-hole tubular structures as an efficient sulfur host (Figure 7d).<sup>[88]</sup> The hollow structure with 3D holes provides not only a large number of channels for intimate interaction between the electrolyte and active sulfur but also an internal area to contain sulfur and polysulfides by physical adsorption (Figure 8d). As a result, with high sulfur loading up to 8.9 mg cm<sup>-2</sup>, the high initial capacity of 1387 mA h g<sup>-1</sup> at 0.2C rate decays to 816 mA h g<sup>-1</sup> after 350 cycles.

As the use of carbon materials as conductive network and sulfur host can effectively improve the electrochemical performance of Li–S batteries, Lu et al. prepared sulfur host materials with excellent electronic transportation capacity and conductivity by combining CNTs with NiCo<sub>2</sub>S<sub>4</sub>.<sup>[89]</sup> The structure of NiCo<sub>2</sub>S<sub>4</sub>@CNTs composites are similar to that of thin branches filled with densely packed small leaves, in which the branches are CNTs and the small leaves are porous flake-shaped NiCo<sub>2</sub>S<sub>4</sub> (Figures 7e and 8e). The NiCo<sub>2</sub>S<sub>4</sub>@CNTs/S composite with higher specific surface area and lower resistance exhibits an initial capacity of 780 mA h g<sup>-1</sup> at 0.6C rate with fading rate of 0.0489% per cycle over 1000 cycles and the columbic efficiency of each cycle is about 99%.

However, most of the hollow tubes and 2D sheet structures of polar metal sulfides are easily damaged during punching and filming process, resulting in the reduction of sulfur utilization. Recently, Yang et al. innovatively synthesized NiCo<sub>2</sub>S<sub>4</sub>, Co<sub>3</sub>S<sub>4</sub>/NiS<sub>2</sub>, and Ni–Co sulfide on Ni-foam (Figure 7f) via one-step hydrothermal synthesis, avoiding the destruction of the

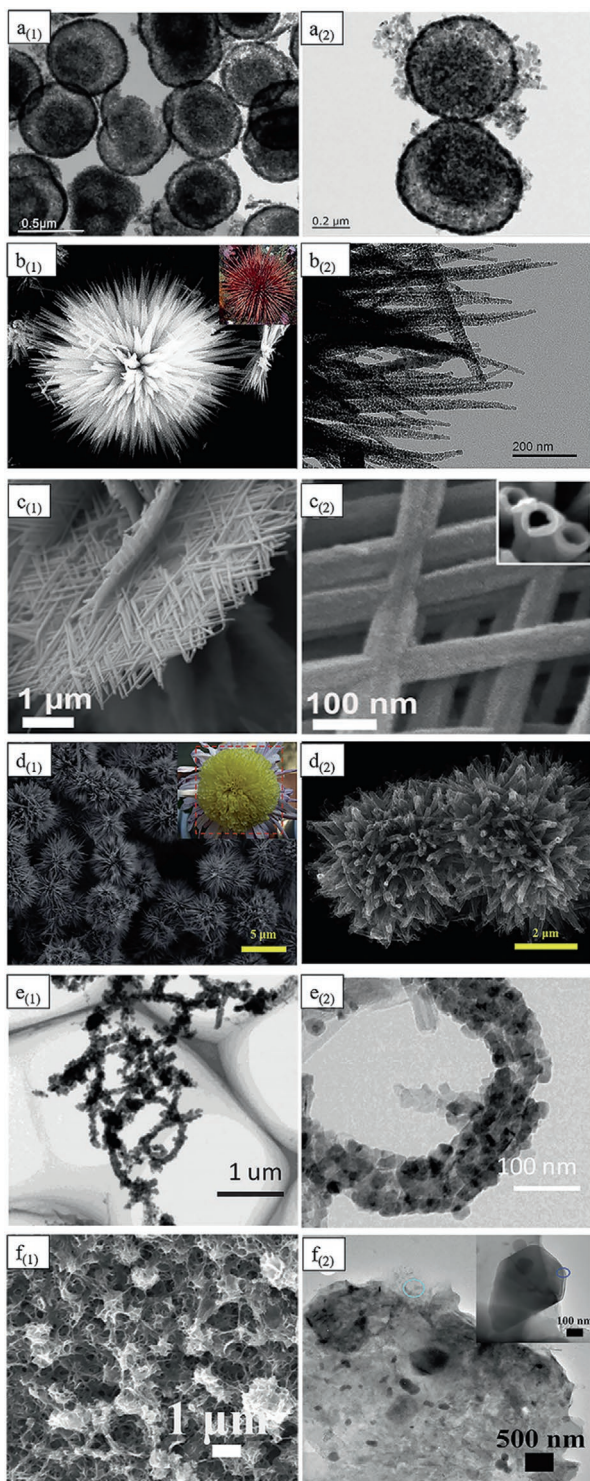


**Figure 7.** SEM and TEM images of  $\text{NiCo}_2\text{S}_4$  as host materials for sulfur. a)  $\text{NiCo}_2\text{S}_4$  spheres. Reproduced with permission.<sup>[85]</sup> Copyright 2019, Springer Nature. b) Urchin-like  $\text{NiCo}_2\text{S}_4$  precursor. Reproduced with permission.<sup>[86]</sup> Copyright 2018, Springer Nature. c) Knot-like  $\text{NiCo}_2\text{S}_4$  matrixes. Reproduced with permission.<sup>[87]</sup> Copyright 2018, Elsevier. d) Self-assembled  $\text{NiCo}_2\text{S}_4$  granules. Reproduced with permission.<sup>[88]</sup> Copyright 2020, Elsevier. e) Thin branches-like  $\text{NiCo}_2\text{S}_4$ @CNTs. Reproduced with permission.<sup>[89]</sup> Copyright 2018, Elsevier. f) NF@NCS-30 nanosheets and the inset of  $\text{Co}_3\text{S}_4$  particle. Reproduced with permission.<sup>[90]</sup> Copyright 2019, Elsevier.

original structure by the reaction process (Figure 8f).<sup>[90]</sup> The electrochemical performance of the foam-like S/Ni-foam@Ni-Co sulfide (S/NF@NCS) delivers an ultrahigh initial capacity of  $1920 \text{ mA h g}^{-1}$  at 0.1C rate, as well as a high capacity of  $1352 \text{ mA h g}^{-1}$  at 1 C after 10 cycles, which decreases to  $\approx 500 \text{ mA h g}^{-1}$  after 100 cycles, showing the poor cycling performance of S/Ni-foam@Ni-Co.

In addition, other nickel–cobalt sulfides similar to  $\text{NiCo}_2\text{S}_4$  can also effectively bind polysulfides and reduce shuttle effect. Recently, Liao et al. had embedded  $\text{Ni}_x\text{Co}_{3-x}\text{S}_4$  nanocrystals with high polarity on a 3D porous nitrogen-doped carbon nanosheet, which promotes efficient utilization of sulfur. It has been proved that the  $\text{Ni}^{2+}$  and  $\text{Co}^{3+}$  sites on  $\text{Ni}_x\text{Co}_{3-x}\text{S}_4$  nanocrystals surface can act synergistically with N sites on N-doped carbon nanosheet in anchoring polysulfides.<sup>[91]</sup> Also, the diffusion barrier of  $\text{Li}^+$  ions at the  $\text{Ni}_x\text{Co}_{3-x}\text{S}_4$ /N-doped graphene interface is much lower than pure  $\text{Ni}_x\text{Co}_{3-x}\text{S}_4$  surface, which means that combining with carbon materials gives composite an overall better reaction kinetics. The obtained composite demonstrates excellent cycle stability by an initial capacity of  $1162 \text{ mA h g}^{-1}$  and low capacity degradation of 0.14% per cycle in 400 cycles at 1C, proving the good anchoring effects of the  $\text{Li}_2\text{S}_n$  on the bimetallic polar materials. Besides the sulfur host, another effective attempt to use  $\text{CoNi}_2\text{S}_4$  as additive was proposed by Bhardwaj et al.<sup>[92]</sup> By simply adding  $\text{CoNi}_2\text{S}_4$  powder to sulfur cathode, the specific capacity of  $\text{CoNi}_2\text{S}_4/\text{S}$  at the end of the first discharge cycle increases to  $1570 \text{ mA h g}^{-1}$ , which is very close to the theoretical capacity of sulfur cathode. After that, although the capacity decreases rapidly to  $1000 \text{ mA h g}^{-1}$  within 10 cycles, it still remains 90% after 100 cycles. Compared with sulfur host materials, this cobalt–nickel sulfide additive effectively makes the assembly of metal–sulfur batteries considerably simpler and promotes the commercialization of sulfur cathode containing bimetallic sulfides.

Similar to  $\text{NiCo}_2\text{O}_4$ , the (311) crystal plane is the main exposed crystal plane in  $\text{NiCo}_2\text{S}_4$  and it has the strongest ability to adsorb polysulfides, in which the high valence Ni and Co ions are the main components that bond with LiPs. The special secondary structure of  $\text{NiCo}_2\text{S}_4$  can also effectively bind the sulfur inside the cathode. However, nickel cobalt sulfides have better conductivity attributed to denser electron atmosphere and unique band structures compared with oxides. As shown in Table 3, because of the electrical conductivity of  $\text{NiCo}_2\text{S}_4$  is  $\approx 100$  times that of  $\text{NiCo}_2\text{O}_4$ , the  $\text{NiCo}_2\text{S}_4$  shows high conductivity even without addition of any carbon material, so it generally has higher sulfur content and initial capacity at high rate when used as sulfur host.<sup>[93]</sup> However, as the sulfur bond is weaker than oxygen bond, the cyclic stability of the S/ $\text{NiCo}_2\text{S}_4$  composite cathodes still need to be improved.

### 3.1.2. $\text{Cu}_3\text{BiS}_3$

Cu–Bi–S composites are very stable at room temperature and are composed of abundant and cheap elements, so  $\text{Cu}_3\text{BiS}_3$  as one of the Cu–Bi–S materials was used by Gao et al. as sulfur host of Li–S batteries to absorb polysulfide.<sup>[94]</sup> The  $\text{Cu}_3\text{BiS}_3$  is synthesized by solvothermal method and has a flower-like structure with a diameter of 1.5–3  $\mu\text{m}$ , which is composed of

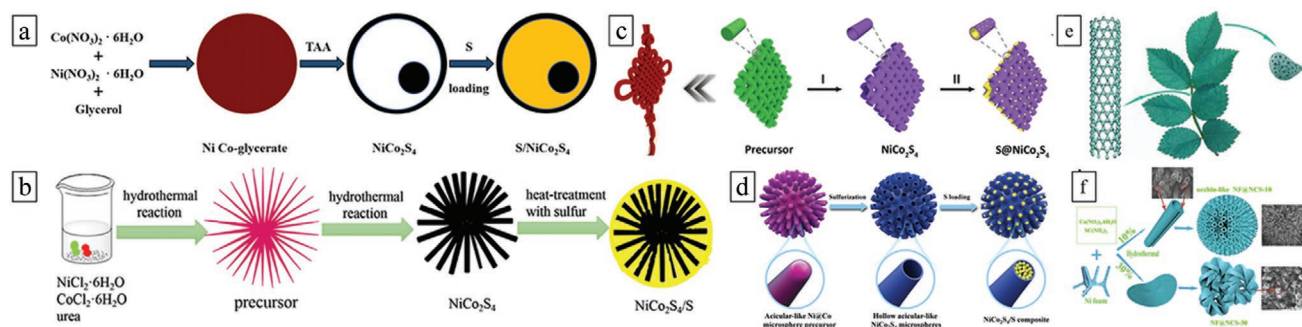


**Figure 8.** The schematic illustrations of the preparation of  $\text{NiCo}_2\text{S}_4\text{-S}$  nanostructures. a)  $\text{S}/\text{NiCo}_2\text{S}_4$  yolk-shell hollow spheres. Reproduced with permission.<sup>[85]</sup> Copyright Springer-Verlag GmbH Germany, part of Springer Nature 2019. b) Urchin-like  $\text{NiCo}_2\text{S}_4/\text{S}$  composites. Reproduced with permission.<sup>[86]</sup> Copyright Springer Science+Business Media, LLC, part of Springer Nature 2018. c) Knot-like  $\text{S}@/\text{NiCo}_2\text{S}_4$  composites. Reproduced with permission.<sup>[87]</sup> Copyright 2018, Elsevier. d) Hollow acicular-like  $\text{NiCo}_2\text{S}_4/\text{S}$  composites. Reproduced with permission.<sup>[88]</sup> Copyright 2020, Elsevier. e) Thin branches-like  $\text{NiCo}_2\text{S}_4@\text{CNTs}$ . Reproduced with permission.<sup>[89]</sup> Copyright 2018, Elsevier. f)  $\text{NF}@\text{NCS-30}$  and  $\text{NF}@\text{NCS-10}$ . Reproduced with permission.<sup>[90]</sup> Copyright 2019, Elsevier.

oriented 2D thin nanosheets, resulting in a junction with porosities between these nanosheets and exhibiting a hierarchical nanostructure.  $\text{Cu}_3\text{BiS}_3/\text{S}$  composite as a cathode with 80 wt% sulfur content exhibits an initial capacity of  $1343 \text{ mA h g}^{-1}$  at 0.2C rate and maintains the capacity of  $487 \text{ mA h g}^{-1}$  after 100 cycles, which shows good electrochemical performance while the cycle performance still needs to be improved.

### 3.1.3. $\text{ZnCo}_2\text{S}_4$

$\text{ZnCo}_2\text{S}_4$  has a similar structure and ability to form polar bonds with polysulfide as  $\text{ZnCo}_2\text{O}_4$ , while  $\text{ZnCo}_2\text{S}_4$  has a smaller Li ion diffusion barrier energy than  $\text{ZnCo}_2\text{O}_4$ , which benefits Li ion transportation during charge-discharge. Thus, Zhang et al. tried to grow  $\text{ZnCo}_2\text{S}_4$  nanoflakes derived from a metal-organic framework (MOF) on conductive carbon cloth as a binder free electrode.<sup>[95]</sup> According to calculations, although  $\text{ZnCo}_2\text{O}_4$  has a higher binding energy than  $\text{ZnCo}_2\text{S}_4$ , it also causes more decomposition of polysulfides. In addition,  $\text{ZnCo}_2\text{S}_4$  exhibited lower bandgap, indicating that Li ions migrate more readily on  $\text{ZnCo}_2\text{S}_4$  than on  $\text{ZnCo}_2\text{O}_4$ . The prepared  $\text{ZnCo}_2\text{S}_4/\text{S}$  delivers an initial capacity of  $1146 \text{ mA h g}^{-1}$  and a capacity of  $531 \text{ mA h g}^{-1}$  at 0.5C after cycling 200 times, while the  $\text{ZnCo}_2\text{O}_4/\text{S}$  cathode shows a capacity of only  $413 \text{ mAh g}^{-1}$  after 200 cycles at 0.5C, proving that the  $\text{ZnCo}_2\text{S}_4/\text{S}$  composite presents a more stable

performance compared with the  $\text{ZnCo}_2\text{O}_4/\text{S}$ . This study shows that the sulfur host materials with appropriate binding energy have better effect of reducing shuttle effect than sulfur host materials with high binding energy.

### 3.2. Selenides

Compared with metal sulfides, the high structural flexibility and inherent metallic properties of metallic selenides bring good cycle performance and good conductivity, which make them promising electrode materials with wide range of application prospects.<sup>[96]</sup>

Due to the synergistic effect of Ni and Co bimetals which can significantly enrich the electronic reaction process and improve the conductivity, Zhang et al. used highly conductive and polar bimetallic selenide  $\text{NiCo}_2\text{Se}_4$  (NCSe) with a tubular structure to prepare urchin-like  $\text{S}/\text{NCSe}$  composites as cathode materials for Li-S battery.<sup>[97]</sup> The  $\text{S}/\text{NCSe}$  composite with low sulfur loading exhibits a reversible capacity of  $480 \text{ mA h g}^{-1}$  at 3C rate with fading rate of 0.016% per cycle after 1000 cycles, and with higher sulfur loading of  $3.2 \text{ mg cm}^{-2}$  exhibits a reversible capacity of  $557 \text{ mA h g}^{-1}$  with fading rate of 0.043% per cycle after 600 cycles, which shows good cycle stability with both high and low sulfur content. In addition, cytotoxicity tests show that NCSe has an excellent biocompatibility. This research not

**Table 3.** Summary of studies on  $\text{NiCo}_2\text{S}_4$  composites with variable secondary structure as cathode materials for lithium-sulfur batteries.

Materials	Initial capacity [mA h g <sup>-1</sup> ]	Current rate <sup>a)</sup>	Cycle number	Degradation rate per cycle [%]	Sulfur content <sup>b)</sup> [wt%]	Rate performance <sup>c)</sup> at 1C [mA h g <sup>-1</sup> ]	Ref.
$\text{NiCo}_2\text{S}_4$ yolk-shell hollow spheres	≈506 <sup>d)</sup>	0.5C	500	0.074	70	387	[85]
Urchin-like $\text{NiCo}_2\text{S}_4$	759	1.0C	300	0.180	45.8	567	[86]
Chinese knot-like $\text{NiCo}_2\text{S}_4$ nanotubes	932	1.0C	1000	0.020	71	926	[87]
Self-assembled $\text{NiCo}_2\text{S}_4$ granules	1387	0.2C	350	0.117 <sup>d)</sup>	67	816	[88]
Foam-like Ni-foam@Ni-Co sulfide	1352	1.0C	100	0.630 <sup>d)</sup>	N/A	430	[90]
Branch-with-leaves-like $\text{NiCo}_2\text{S}_4@\text{CNTs}$ <sup>d)</sup>	780	0.6C	1000	≈0.049	66	660 (at 1.2C)	[89]

<sup>a)</sup>1C =  $1674 \text{ mA g}^{-1}$ ; <sup>b)</sup>Mass percentage of sulfur on the whole cathode; <sup>c)</sup>Capacity of cathode at various C-rate; <sup>d)</sup>Data is estimated from the figure given by paper since authors did not provide the specific value in the reference; <sup>e)</sup>CNTs = carbon nanotubes.

only expands the application of metal selenides, but also provides a new strategy for the preparation of long-life and high-rate Li–S batteries.

Due to the lower bond energy of metal sulfur bond and metal selenium bond compared with metal oxygen bond, transition metal sulfides and selenides have better structural flexibility and worse structural stability than metal oxides, therefore, when used as host materials, they generally have higher initial capacity and poor cycle stability. Moreover, their various microstructures benefiting from structural flexibility have led to a growing number of studies on them in recent years.

## 4. Others

### 4.1. Mo<sub>3</sub>Ni<sub>3</sub>N

Metal carbides as sulfur host materials have physical/chemical absorptivity similar to that of metal oxides but conductivity much higher than that of oxides, but the low sulfur loading (<2.0 mg cm<sup>-2</sup>) and serious shuttle effect caused by the weak polysulfide binding ability. In order to solve this problem, Liu et al. used branch-like Mo<sub>3</sub>Ni<sub>3</sub>N/Mo<sub>2</sub>C nanoparticles anchors on carbonized bacterial cellulose film (CBC) to prepare a kind of free-standing 3D carbon/inorganic multi-component matrix as sulfur host material for Li–S batteries, in which 1D CBC fibers form a porous highly conductive network.<sup>[98]</sup> Mo<sub>2</sub>C is mainly used to enhance its conductivity and Mo<sub>3</sub>Ni<sub>3</sub>N can effectively bind the dissolved polysulfide. The cathode containing hybrid material of Mo<sub>3</sub>Ni<sub>3</sub>N/Mo<sub>2</sub>C-CBC/S membrane not only achieves 70 wt% sulfur content with area sulfur loading of 15.5 mg cm<sup>-2</sup>, but also exhibits the initial capacity of 823 mA h g<sup>-1</sup> at 1C rate and reversible capacity of 519 mA h g<sup>-1</sup> after 500 cycles. On the other hand, the cathode without Mo<sub>3</sub>Ni<sub>3</sub>N exhibits much lower capacity, which proves that Mo<sub>3</sub>Ni<sub>3</sub>N plays an important role for better battery performance.

### 4.2. Prussian Blue (MOF)

As an alternative to sulfur-based materials, the large number of open coordination metal sites in MOF materials act as soft Lewis acids that can effectively coordinate polysulfide anions through Lewis acid–base bonding effect. However, the poor conductivity of MOF gets it less attention. Prussian blue analog (PBA) is a porous coordination polymer with a large open framework for sulfur storage, which is similar to MOF. Su et al. used PBAs as sulfur host of Li–S batteries by combining Na<sub>2</sub>Fe[Fe(CN)<sub>6</sub>] with conductive polymer poly(3,4-ethylenedioxythiophene) (PEDOT).<sup>[99]</sup> Na<sub>2</sub>Fe[Fe(CN)<sub>6</sub>] nanoparticles have a cubic morphology with highly uniform size of ≈150 nm, in which iron ions are in the center of Fe[Fe(CN)<sub>6</sub>]<sup>2-</sup> and are coordinated by six cyanate radicals to form octahedrons. The inserted sulfur occupies only the large interstitial sites rather than the external surface of the Na<sub>2</sub>Fe[Fe(CN)<sub>6</sub>] nanocrystals, avoiding the blocking of electrical current transporting paths and resulting in a higher sulfur content (82 wt%). The S@Na<sub>2</sub>Fe[Fe(CN)<sub>6</sub>]@PEDOT composite delivers a high initial capacity of 1291 mA h g<sup>-1</sup> at 0.1C rate and remained at

1101 mA h g<sup>-1</sup> after 100 cycles, while the revisable capacity of S@Na<sub>2</sub>Fe[Fe(CN)<sub>6</sub>] cathode only remains at 763 mA h g<sup>-1</sup> after 100 cycles at 0.1C rate, which shows that PEDOT coating layer could greatly accelerate the electron transport, resulting in Li<sup>+</sup> ion diffusion and therefore improving the cyclability of battery. This study provides a new idea for the application of PBAs and MOF in the cathode of Li–S battery.

### 4.3. LiFePO<sub>4</sub>

Olivine-type LiFePO<sub>4</sub> (LFP) is widely used as a host material in lithium-ion battery due to its high theoretical capacity (about 170 mA h g<sup>-1</sup>), acceptable operating voltage, low cost, low toxicity, and thermal stability. The results show that (010) planes of LFP have 1D Li<sup>+</sup> diffusion channels and therefore lower Li migration energy and higher Li diffusion coefficient, which gives the LFP better rate capability. When LFP is applied in Li–S batteries, it exhibits an emerging metallic property at the LFP/Li<sub>2</sub>S interface with improved electronic conductivity, as well as excellent polar property and high redox potential, making it a potential sulfur host material.<sup>[100,101]</sup> However, the application of LFP as the electrode materials for lithium–sulfur battery is limited.

Kim et al. first coated the sulfur with a layer of LFP through mechano-fusion technique, avoiding multi-step solution processes commonly used to make sulfur composites, improving the specific gravity and sulfur content of cells, so the volumetric energy density also increases accordingly.<sup>[102]</sup> The as-prepared S-LFP composite exhibits a capacity of 1200 mA h g<sup>-1</sup> at 0.1C rate, which is higher than the pristine sulfur electrode, as well as a high specific energy and energy density. Lee et al. used nanosized LiFePO<sub>4</sub> as a hard template to design triple-heteroatom (P, O, and N)-doped hollow carbon-on-graphene nanosheets (PONHC/G), which have a high surface area (655.2 m<sup>2</sup> g<sup>-1</sup>), efficient active sites, and excellent conductivity given by graphite nanosheets.<sup>[103]</sup> The S@PONHC/G cathode exhibits a higher initial capacity of 825 mA h g<sup>-1</sup> at 1C rate, which decreases to 711 mA h g<sup>-1</sup> after 200 cycles and to 607 mA h g<sup>-1</sup> after 500 cycles. The result proves that LFP as a sulfur host can provide effective physical sulfur binding (sulfur content ≈70 wt%) and considerable chemical affinity with LiPSs. Recently, Wang et al. reduced the shuttle effect and optimized the electrochemical reaction process by combining LFP and holey graphene (HG) to fabricate the HG/LFP/S cathode composites with a yolk–shell structure, which provide both physical and chemical absorption for LiPSs.<sup>[104]</sup> The HG/LFP/S cathode with a unique heterostructure (74.7% sulfur content) provides an initial capacity of 1066 mA h g<sup>-1</sup> at 1C rate and a reversible capacity of 831 mA h g<sup>-1</sup> after 500 cycles with the fading rate of 0.044% per cycle, which exhibits impressive rate and cycling performance compared with 483 mA h g<sup>-1</sup> of HG/S electrode without LFP nanoparticles after 500 cycles at 1C rate. The excellent electrochemical properties of LFP make it attractive for researchers, but its low conductivity often limits its further application. In order to solve this problem, LFP is usually combine with conductive carbon materials to provide high conductivity and fast electron's transportation as well as a beneficial synergistic effect by forming heterostructure with carbon materials.

#### 4.4. NiCoP

Metal phosphides have better electrical conductivity than their oxides and sulfides counterparts, and some of them even have superconductivity, which facilitates redox reaction kinetics and increases sulfur utilization. Moreover, the synthesis of phosphide is much simpler than that of nitride or carbide. However, the application of metal–phosphide materials has been limited by its low surface area and areal sulfur loading.<sup>[105]</sup> Recently, Duan et al. prepared metal phosphide NiCoP with hollow quasi-polyhedron structure by acid etching method to load sulfur, in which the open and fold architecture as a nanoscale reservoir can effectively provide physical adsorption for polysulfides.<sup>[106]</sup> In addition, the oxide layer on the surface of NiCoP nanoparticles can activate Ni/Co sites to chemically bind polysulfides in electrolyte. A large discharge capacity of 815.3 mA h g<sup>-1</sup> in the initial cycle at 0.1C is obtained by NiCoP/S composite cathode with 70 wt% sulfur, and maintains at 620.1 mA h g<sup>-1</sup> after 200 cycles. The study also proves that P atoms can regulate the interfacial electron transfer dynamics and synergistically improve the electrochemical performance of sulfur cathode with transition metal ions.

### 5. Mechanism

The most conventional technique to suppress the dissolved LiPSs species is “physical adsorption.” Although the physically composite sulfur with conductive materials can trap the LiPSs, but it is inevitable that the impregnated sulfur can still be get into the electrolyte because of the penetration effect. During the lithiation process, the highly soluble LiPSs can diffuse across the physical barrier since weak interactions between host materials and LiPSs can only hold for a short time.<sup>[107–110]</sup> Because of the weak van der Waals force, the physical absorption method cannot restrict the long-term diffusion of LiPSs and the LiPSs cannot efficiently be combined with the host materials due to the strong electric field of the driving force for the diffusion of LiPSs and therefore, the host active materials loss which cause the serious polysulfides shuttle effect.<sup>[111–113]</sup> A novel type of compounds have been developed which provides chemisorption on sulfur species that can inhibits the diffusion of lithium polysulfide species. Sulfur species are covalently bonded to the host materials, by reacting with the functional groups on the surface to completely stop the diffusion of LiPSs. This is so-called “chemical adsorption.”<sup>[113]</sup> The “chemical adsorption” significantly helps to suppress the diffusion of LiPSs and can be held within the cathode via strong chemical bonds, therefore the polysulfides shuttle can be efficiently eliminated which improve the cycle stability and columbic efficiency. Simply, the key difference is that the “physical adsorption” method is based on van der Waals force that usually forms a multi-molecular layer and “chemical adsorption” method is based on chemical bonding force that can form a mono-molecular layer on the surface.<sup>[114]</sup> Lewis acid–base interaction could be an alternative strategy which is introduced for a chemical and structural synergistic immobilization of polysulfides.<sup>[115–117]</sup> One approach that leads to an occupied lower energy level, accounts covalent interaction between the highest occupied molecular orbital of

a Lewis base and lowest occupied molecular orbital of a Lewis acid.<sup>[115]</sup> This level is considered to be a combination of the highest occupied molecular orbital of the Lewis base and the lowest occupied molecular orbital of the Lewis acid which lead to an effective charge transfer from Lewis base to Lewis acid (Figure 9a).<sup>[118]</sup> Another strategy to suppress the higher order dissolution polysulfides is polar–polar interactions.<sup>[118–120]</sup> The polar bonds exist in the polar molecules due to the difference in electronegativity between the bonded atoms. The interaction between polar molecules by dipole-dipole intermolecular forces and hydrogen bonds which is much stronger than the interaction between polar and nonpolar molecule. The chemical affinity in polar–polar interaction with respect to anchoring Li<sub>2</sub>S<sub>n</sub> species is more favorable. The polar materials show strong interaction with polysulfides without any doping due to intrinsic polarity, absorbing polar polysulfides, and suppressing shuttle effect.<sup>[119]</sup> The polar materials owing to their stronger interactions with polar polysulfides and share positive attributes that contribute to enhanced electrochemical performance of the Li–S batteries. The polar materials have not only strong ability to absorb and trap the polysulfides to suppress the shuttle effect but also proven to accelerate the transformation process between lithium polysulfide and polysulfide because of their higher reactivity and large surface sites. All these features provide better stability, improved reversibility, and longer lifespan for Li–S batteries (Figure 9b).<sup>[118]</sup> During lithiation the dissolved lithium polysulfides themselves can also be used as a cathode, and their high solubility is attractive for a new type of flow battery. However, it is necessary to induce precipitation of solid to obtain high capacity in nonaqueous solvents. Due to insulating nature of Li<sub>2</sub>S, a conductive material is added to facilitate the charge transfer and provide a substrate for the electrodeposition reactions. Through nucleation and growth, the Li<sub>2</sub>S precipitation on conductive substrates takes place by the reduction of the polysulfide at three boundary stages between the existing Li<sub>2</sub>S precipitate, conductive substrate, and solution phase. Nucleation needs higher driving force than growth, since surface energy barriers must be overcome. In electrodeposition, lower energy barrier for growth than for nucleation is expected which has been observed for the precipitation of Li<sub>2</sub>O<sub>2</sub> in lithium–oxygen batteries.<sup>[121]</sup> The length of these three boundary stages reaches a maximum during nucleation and growth which vanishes when the precipitates fully impinged. Because of the conductivity limitation, the thickness growth cannot occur by bulk chemical diffusion via Li<sub>2</sub>S layer, but occurs through surface diffusion at Li<sub>2</sub>S–electrolyte interface and the Li<sub>2</sub>S thickness is depend on the total growth time available. For electrodeposited materials, the current instead increases monotonically and asymptotically reaches a maximum value that assumes no diffusion limitation.<sup>[122–124]</sup> Depending on the current rate, the Li<sub>2</sub>S precipitation produces different morphologies which in turn determines over potential. Large over potentials produce a high nuclei density at high C-rates, so the continuous morphology composed of various small crystallites is obtained but Lower C-rates produce fewer but larger precipitates. Through Li<sub>2</sub>S precipitation, the high storage capacities can be realized by controlling the surface area of conductive substrate, choice of solvent, and proper electro-kinetic control of the nucleation and growth process.<sup>[119]</sup> The lithium bond between LiPSs and

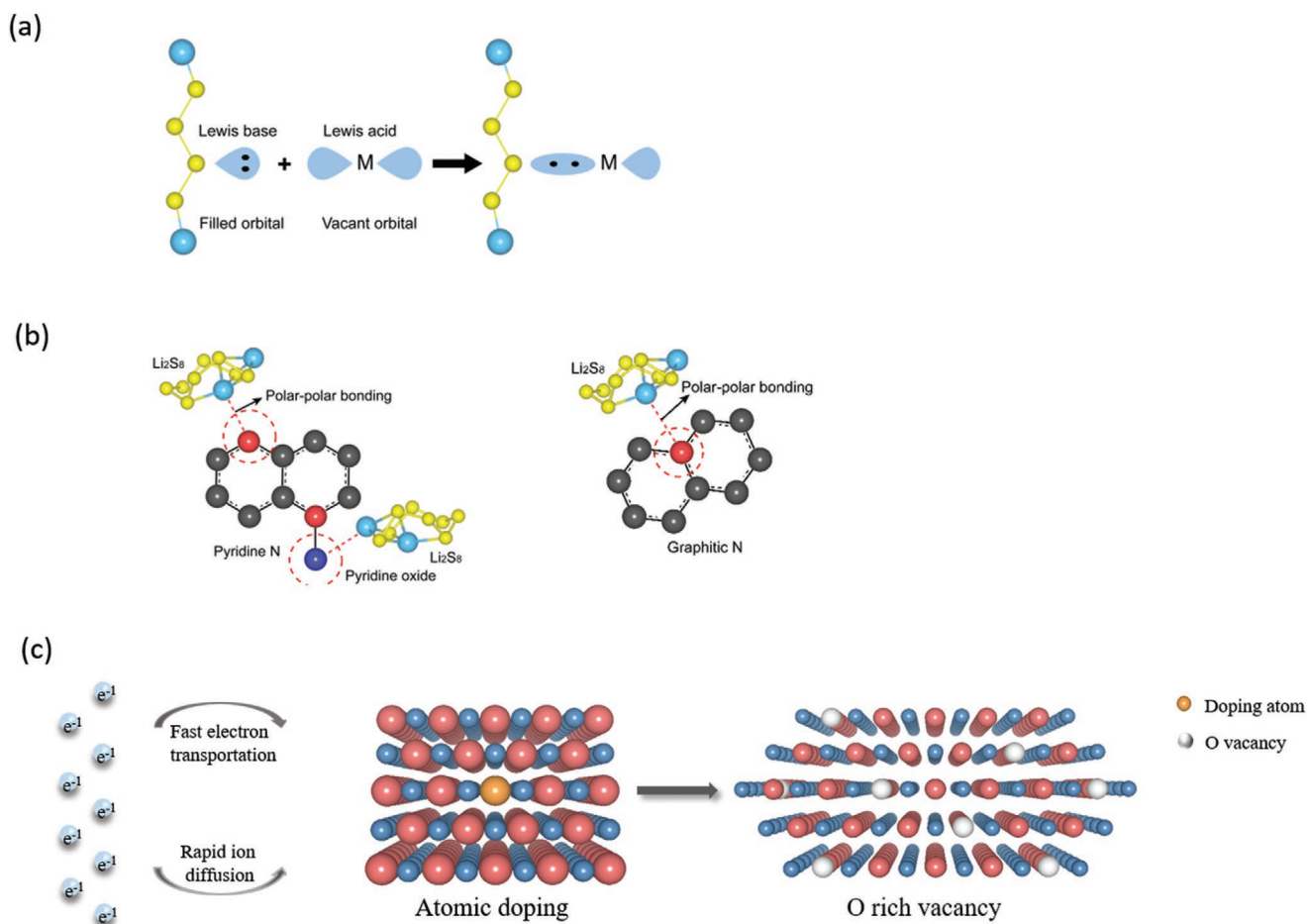


**Figure 9.** a) Lewis acid–base interaction. Reproduced with permission.<sup>[130]</sup> Copyright 2019, Elsevier. b) Polar–polar interactions. c) The uniform atomic doping of B ions in the oxide host assures fast electrical conduction, while the creation of O rich vacancy enables easy access of oxygen ions into the oxide host with a low energy barrier.

lithiophilic surface has well established via polar–polar interactions. Integration of multi-metal components in one crystal is highly expected to tune transportation of LiPSs and regulate the lithium sulfide ( $\text{Li}_2\text{S}$ ) deposition simultaneously.<sup>[125]</sup> Such configuration of material design and mechanistic understanding are fruitful for sulfur hosts.

As compared with simple metal oxides, the multi-metal components encompass rich oxygen vacancies and improve the surface interactions (Figure 9c).<sup>[126]</sup> These oxygen vacancies enhance the metal activity and the oxygen component shows lithiophilic site to bind the LiPSs that provides stable operation of lithium–sulfur batteries. The multi-metal components expose abundant active sites and the highly catalytic nature of multi-metal components loaded on the conductive surface that facilitate the redox kinetic reactions of the LiPSs. Multi-metal components introduce variable and highly valence transition metal ions which regulates the redox kinetic reactions between LiPSs and  $\text{Li}_2\text{S}$  that enhance the electrochemical performance of lithium–sulfur batteries. Also, the higher tap density of the multi-metal compound confers a higher volumetric capacity of sulfur cathode compared to carbon materials (Table 4). Due to their unique ferroelectric, piezoelectric, and ferroelastic properties, the multiferroelectric materials also provides a novel

polysulfide trapping strategy to conquer the polysulfide shuttle effect.<sup>[127]</sup> For photovoltaic and photocatalysis, the ferroelectricity “spontaneous polarization,” caused by asymmetric crystal structure, offers new opportunities.<sup>[128]</sup> The “spontaneous polarization” is helpful to build an internal EF and induces charges on the surface of ferroelectric materials, resulting in a plenty of polar molecules from the outside will be chemisorbed on the surface of ferroelectric materials to screen these surface charges.<sup>[129]</sup> The heteropolar polysulfides can be anchored because of the originated EF from the “spontaneous polarization” of ferroelectrics that is important to solve the shuttle effect problem. There is another strategy which is called “bottom-up strategy.” Multifunctional 3D polar composite electrode which is established via in situ epitaxial growth is a viable methodology to provide both LiPSs immobilization and conversion capabilities to alleviate the shuttle effect as well as improve the electrochemical performance of lithium–sulfur batteries.

## 6. Conclusion and Outlook

In conclusion, we systematically discussed strategies and recent development in multi-metal-based compounds as host materials

**Table 4.** Summary of studies about the high volumetric capacity of multi-metal oxides and its comparison with carbon materials.

Materials	Initial capacity [mA h g <sup>-1</sup> ]	Current rate <sup>a)</sup>	Tap density [g cm <sup>-3</sup> ]	Volumetric capacity [mA h cm <sup>-3</sup> ]	Ref.
NiCo <sub>2</sub> O <sub>4</sub> nanofibers	872	0.5C	1.66	1447	[41]
NiFe <sub>2</sub> O <sub>4</sub> nanofibers	963.6	0.1C	1.33	1281.7	[47]
NCM811 microspheres	1264.3	0.1C	1.81	1601.9	[75]
La <sub>0.8</sub> Sr <sub>0.2</sub> MnO <sub>3</sub> nanofibers	792	0.1C	1.69	1338.5	[68]
Carbon nanofibers	654	0.5C	0.96	628	[41]
Carbon nanotubes	1044.3	0.1C	0.64	668.4	[47]

<sup>a)</sup>1C = 1674 mA g<sup>-1</sup>.

to demonstrate the main parameters related with polysulfide adsorption capability and energy barriers of lithium–sulfur batteries. For better electrochemical performance, researchers have developed different structures and morphologies of multi-metal-based compounds that could efficiently constrain the dissolution of polysulfides into liquid electrolyte and volume expansion during discharge process. Furthermore, the multi-metal-based compounds as cathode material for lithium–sulfur batteries show lower over-potential, higher energy density, better cycling stability, and improved columbic efficiency. The intrinsic metallic conductivity and reduction–oxidation catalyzing ability facilitate the transportation of Li ion and strong interaction with LiPSs, and accelerated surface redox reaction of multi-metal-based compounds are critical to reduce energy barrier and improve the battery performance.

There are still many challenges to fabricate the sulfur-based cathode materials for lithium–sulfur batteries to fulfill all practical requirements. To fully exploit, it is critical for researchers to optimize the synthesis parameters as well as material properties. Here some recommendations are summarized that may provide deeper insights and pathways for the development of sulfur host materials of lithium–sulfur batteries.

- i) For practical applications, low cost materials should be selected. Naturally abundant organic molecules and non-noble metal compounds can be considered.
- ii) The gravimetric fractions of electrode-based materials should be minimized. In the range of operating voltage, some materials are electrochemically inactive and decrease the gravimetric energy density. Thus, an optimized point is required to maximize the energy density.
- iii) More work emphasized for the fabrication of novel structures and morphologies to confine LiPSs and further improve the electrochemical activities. The design of materials should be based on a mechanistic understanding of different parameters. In catalytic activities, the adsorption energy effect with LiPSs, electrical conductivity, diffusivity of the lithium ion (Li<sup>+</sup>) and the coordination of unsaturated atoms should be further considered.
- iv) Current applied approaches for the fabrication of electrode–materials were limited to some classical methods. Thus, a deeper understanding of electrocatalytic interaction and chemical anchoring should be required by combining electrochemical testing with advanced in situ characterization methods, like X-ray powder diffraction (XRD), X-ray

photoelectron spectroscopy (XPS), Raman spectroscopy, and microscopy techniques.

## Acknowledgements

Y.-C.J. and H.M.U.A. contributed equally to this work. Financial support from the New Energy Project for Electric Vehicles in National Key Research and Development Program (2016YFB0100200) and the NSFC (21935006 and 21421001) of China are gratefully acknowledged.

## Conflict of Interest

The authors declare no conflict of interest.

## Keywords

cathodes, host materials, lithium–sulfur batteries, multi-metallic compounds

Received: August 29, 2020

Revised: October 28, 2020

Published online:

- [1] M. Wild, L. O'Neill, T. Zhang, R. Purkayastha, G. Minton, M. Marinescu, G. J. Offer, *Energy Environ. Sci.* **2015**, *8*, 3477.
- [2] P. G. Bruce, S. A. Freunberger, L. J. Hardwick, J.-M. Tarascon, *Nat. Mater.* **2012**, *11*, 19.
- [3] X. Ji, L. F. Nazar, *J. Mater. Chem.* **2010**, *20*, 9821.
- [4] X. Fan, W. Sun, F. Meng, A. Xing, J. Liu, *Green Energy Environ.* **2018**, *3*, 2.
- [5] S.-H. Chung, C.-H. Chang, A. Manthiram, *Adv. Funct. Mater.* **2018**, *28*, 1801188.
- [6] Z. W. Seh, Y. Sun, Q. Zhang, Y. Cui, *Chem. Soc. Rev.* **2016**, *45*, 5605.
- [7] M.-K. Song, E. J. Cairnsb, Y. Zhang, *Nanoscale* **2013**, *5*, 2186.
- [8] S. Waluś, G. Offer, I. Hunt, Y. Patel, T. Stockley, J. Williams, R. Purkayastha, *Energy Storage Mater.* **2018**, *10*, 233.
- [9] A. Manthiram, Y. Fu, S.-H. Chung, C. Zu, Y.-S. Su, *Chem. Rev.* **2014**, *114*, 11751.
- [10] K. Zhu, C. Wang, Z. Chi, F. Ke, Y. Yang, A. Wang, W. Wang, L. Miao, *Front. Energy Res.* **2019**, *7*, 123.
- [11] M. Wang, X. Xia, Y. Zhong, J. Wu, R. Xu, Z. Yao, D. Wang, W. Tang, X. Wang, J. Tu, *Chem. - Eur. J.* **2018**, *25*, 3710.
- [12] Z. Li, J. T. Zhang, Y. M. Chen, J. Li, X. W. Lou, *Nat. Commun.* **2015**, *6*, 8850.

- [13] B. Liu, K. Fan, J. Li, G. Liu, Y. Liu, C. Yang, H. Tong, K. Han, D. Qian, *Mater. Res. Bull.* **2020**, *121*, 110625.
- [14] A. C. Juhl, A. Schneider, B. Ufer, T. Brezesinski, J. Janek, M. Fröba, *Beilstein J. Nanotechnol.* **2016**, *7*, 1229.
- [15] P. Wu, H.-Y. Hu, N. Xie, C. Wang, F. Wu, M. Pan, H.-F. Li, X.-D. Wang, Z. Zeng, S. Deng, G.-P. Dai, *RSC Adv.* **2019**, *9*, 32247.
- [16] X.-Q. Zhang, C. Liu, Y. Gao, J.-M. Zhang, Y.-Q. Wang, *Nano.* **2020**, *15*, 2030002.
- [17] G. Zhou, E. Paek, G. S. Hwang, A. Manthiram, *Nat. Commun.* **2015**, *6*, 7760.
- [18] L. Wang, Z. Dong, D. Wang, F. Zhang, J. Jin, *Nano Lett.* **2013**, *13*, 6244.
- [19] Z. Wang, Y. Dong, H. Li, Z. Zhao, H. B. Wu, C. Hao, S. Liu, J. Qiu, X. W. Lou, *Nat. Commun.* **2014**, *5*, 5002.
- [20] X. Liang, C. Y. Kwok, F. Lodi-Marzano, Q. Pang, M. Cuisinier, H. Huang, C. J. Hart, D. Houtarde, K. Kaup, H. Sommer, T. Brezesinski, J. Janek, L. F. Nazar, *Adv. Energy Mater.* **2016**, *6*, 1501636.
- [21] Z. W. Seh, W. Li, J. J. Cha, G. Zheng, Y. Yang, M. T. McDowell, P.-C. Hsu, Y. Cui, *Nat. Commun.* **2013**, *4*, 1331.
- [22] Y. Tao, Y. Wei, Y. Liu, J. Wang, W. Qiao, L. Ling, D. Long, *Energy Environ. Sci.* **2016**, *9*, 3230.
- [23] T. Lei, W. Chen, J. Huang, C. Yan, H. Sun, C. Wang, W. Zhang, Y. Li, J. Xiong, *Adv. Energy Mater.* **2016**, *7*, 1601843.
- [24] D.-R. Deng, T.-H. An, Y.-J. Li, Q.-H. Wu, M.-S. Zheng, Q.-F. Dong, *J. Mater. Chem. A* **2016**, *4*, 16184.
- [25] Z. Sun, J. Zhang, L. Yin, G. Hu, R. Fang, H.-M. Cheng, F. Li, *Nat. Commun.* **2017**, *8*, 14627.
- [26] J. Shen, X. Xu, J. Liu, Z. Liu, F. Li, R. Hu, J. Liu, X. Hou, Y. Feng, Y. Yu, M. Zhu, *ACS Nano* **2019**, *13*, 8986.
- [27] Y. Zhong, L. Yin, P. He, W. Liu, Z. Wu, H. Wang, *J. Am. Chem. Soc.* **2018**, *140*, 1455.
- [28] L. Luo, S.-H. Chung, H. Y. Asl, A. Manthiram, *Adv. Mater.* **2018**, *30*, 1804149.
- [29] X. Zeng, X. Gao, G. Li, M. Sun, Z. Lin, M. Ling, J. Zheng, C. Liang, *J. Mater. Chem. A* **2018**, *6*, 17142.
- [30] X. Tao, J. Wang, C. Liu, H. Wang, H. Yao, G. Zheng, Z. W. Seh, Q. Cai, W. Li, G. Zhou, C. Zu, Y. Cui, *Nat. Commun.* **2016**, *5*, 11203.
- [31] S. Chen, J. Zhu, X. Wu, Q. Han, X. Wang, *ACS Nano* **2010**, *4*, 2822.
- [32] N. Yan, L. Hu, Y. Li, Y. Wang, H. Zhong, X. Hu, X. Kong, Q. Chen, *J. Phys. Chem. C* **2012**, *116*, 7227.
- [33] K. Liang, X. Tang, W. Hu, *J. Mater. Chem.* **2012**, *22*, 11062.
- [34] H. Gao, S. Liu, Y. Li, E. Conte, Y. Cao, *Energies* **2017**, *10*, 1787.
- [35] Y. He, W. Chen, X. Li, Z. Zhang, J. Fu, C. Zhao, E. Xie, *ACS Nano* **2013**, *7*, 174.
- [36] L. Kong, X. Chen, B.-Q. Li, H.-J. Peng, J.-Q. Huang, J. Xie, Q. Zhang, *Adv. Mater.* **2018**, *30*, 1705219.
- [37] M. Yu, J. Chen, J. Liu, S. Li, Y. Ma, J. Zhang, J. An, *Electrochim. Acta* **2015**, *151*, 99.
- [38] C. Zhang, S. Bhojate, C. Zhao, P. K. Kahol, N. Kostoglou, C. Mitterer, S. J. Hinder, M. A. Baker, G. Constantinides, K. Polychronopoulou, C. Rebholz, R. K. Gupta, *Catalysts* **2019**, *9*, 176.
- [39] J. Bhattacharya, C. Wolverton, *Phys. Chem. Chem. Phys.* **2013**, *15*, 6486.
- [40] A. Iqbal, Z. Ali Ghazi, A. Muqsit Khattak, A. Ahmad, *J. Solid State Chem.* **2017**, *256*, 189.
- [41] Y. T. Liu, D. D. Han, L. Wang, G. R. Li, S. Liu, X. P. Gao, *Adv. Energy Mater.* **2019**, *9*, 1803477.
- [42] D. Ouyang, J. Xiao, F. Ye, Z. Huang, H. Zhang, L. Zhu, J. Cheng, W. C. H. Choy, *Adv. Energy Mater.* **2018**, *8*, 1702722.
- [43] D. Luo, G. Li, Y. P. Deng, Z. Zhang, J. Li, R. Liang, M. Li, Y. Jiang, W. Zhang, Y. Liu, W. Lei, A. Yu, Z. Chen, *Adv. Energy Mater.* **2019**, *9*, 1900228.
- [44] D. Xiao, H. Zhang, C. Chen, Y. Liu, S. Yuan, C. Lu, *ChemElectroChem* **2017**, *4*, 2959.
- [45] X. Zhang, Y. Fan, M. A. Khan, H. Zhao, D. Ye, J. Wang, B. Yue, J. Fang, J. Xu, L. Zhang, J. Zhang, *Batteries Supercaps* **2019**, *3*, e1900121.
- [46] L. Hu, C. Dai, H. Liu, Y. Li, B. Shen, Y. Chen, S.-J. Bao, M. Xu, *Adv. Energy Mater.* **2018**, *8*, 1800709.
- [47] F. Xu, B. Jin, H. Li, W. Ju, Z. Wen, Q. Jiang, *New J. Chem.* **2019**, *43*, 18294.
- [48] H. Xu, X. Wang, H. Liu, J. Wang, X. Dong, G. Liu, W. Yu, Y. Yang, H. Zhang, *J. Mater. Sci.* **2018**, *53*, 15631.
- [49] Z. Zhang, S. Basu, P. Zhu, H. Zhang, A. Shao, N. Koratkar, Z. Yang, *Carbon* **2019**, *142*, 32.
- [50] Q. Fan, W. Liu, Z. Weng, Y. Sun, H. Wang, *J. Am. Chem. Soc.* **2015**, *137*, 12946.
- [51] H. Wang, N. Zhang, Y. Li, P. Zhang, Z. Chen, C. Zhang, X. Qiao, Y. Dai, Q. Wang, S. Liu, *J. Phys. Chem. Lett.* **2019**, *10*, 6518.
- [52] Z. Zhang, D.-H. Wu, Z. Zhou, G.-R. Li, S. Liu, X.-P. Gao, *Sci. China Mater.* **2018**, *62*, 74.
- [53] T. W. Kim, M. A. Woo, M. Regis, K. S. Choi, *J. Phys. Chem. Lett.* **2014**, *5*, 2370.
- [54] Y. Shi, Y. Zhu, B. Yu, Z. Gui, S. She, R. K. K. Yuen, H. Liu, Y. Hu, *RSC Adv.* **2015**, *5*, 41835.
- [55] B. Liu, J. Zhang, X. Wang, G. Chen, D. Chen, C. Zhou, G. Shen, *Nano Lett.* **2012**, *12*, 3005.
- [56] B. Liu, B. Liu, Q. Wang, X. Wang, Q. Xiang, D. Chen, G. Shen, *ACS Appl. Mater. Interfaces* **2013**, *5*, 10011.
- [57] F. Wang, X. Wang, D. Liu, J. Zhen, J. Li, Y. Wang, H. Zhang, *ACS Appl. Mater. Interfaces* **2014**, *6*, 22216.
- [58] S. Wang, Z. Ding, X. Wang, *Chem. Commun.* **2015**, *51*, 1517.
- [59] Q. Sun, B. Xi, J.-Y. Li, H. Mao, X. Ma, J. Liang, J. Feng, S. Xiong, *Adv. Energy Mater.* **2018**, *8*, 1800595.
- [60] P. Tan, M. Liu, Z. Shao, M. Ni, *Adv. Energy Mater.* **2017**, *7*, 1602674.
- [61] H. Zhu, P. Zhang, H. Dai, *ACS Catal.* **2015**, *5*, 6370.
- [62] L. Wang, M. R. Cho, Y. J. Shin, J. R. Kim, S. Das, J. G. Yoon, J. S. Chung, T. W. Noh, *Nano Lett.* **2016**, *16*, 3911.
- [63] J. Briscoe, S. Dunn, *Adv. Mater.* **2016**, *28*, 3802.
- [64] K. Xie, Y. You, K. Yuan, W. Lu, K. Zhang, F. Xu, M. Ye, S. Ke, C. Shen, X. Zeng, X. Fan, B. Wei, *Adv. Mater.* **2017**, *29*, 1604724.
- [65] H. E. Wang, K. Yin, X. Zhao, N. Qin, Y. Li, Z. Deng, L. Zheng, B. L. Su, Z. Lu, *Chem. Commun.* **2018**, *54*, 12250.
- [66] R. Cohen, *Nature* **1992**, *358*, 136.
- [67] Z. Hao, R. Zeng, L. Yuan, Q. Bing, J. Liu, J. Xiang, Y. Huang, *Nano Energy* **2017**, *40*, 360.
- [68] Y. T. Liu, S. Liu, G. R. Li, T. Y. Yan, X. P. Gao, *Adv. Sci.* **2020**, *7*, 1903693.
- [69] M. Chen, W. Xu, S. Jamil, S. Jiang, C. Huang, X. Wang, Y. Wang, H. Shu, K. Xiang, P. Zeng, *Small* **2018**, *14*, 1803134.
- [70] M. Broussely, F. Perton, P. Biensan, J. M. Bodet, J. Labat, A. Lecerf, *J. Power Sources* **1995**, *54*, 109.
- [71] I. Suzuki, T. Omata, *Semicond. Sci. Technol.* **2017**, *32*, 0130007.
- [72] C. Julien, S. Gastro-Garcia, *J. Power Sources* **2001**, *97–98*, 290.
- [73] J. W. Fergus, *J. Power Sources* **2010**, *195*, 939.
- [74] L. Wang, Y. H. Song, B. H. Zhang, Y. T. Liu, Z. Y. Wang, G. R. Li, S. Liu, X. P. Gao, *ACS Appl. Mater. Interfaces* **2020**, *12*, 5909.
- [75] K. Shi, C. Lai, X. Liu, Y. Wei, W. Lv, J. Wang, J. Li, C. Yan, B. Li, Q.-H. Yang, F. Kang, Y.-B. He, *Energy Storage Mater.* **2019**, *17*, 111.
- [76] R. Ponraj, A. G. Kannan, J. H. Ahn, D. W. Kim, *ACS Appl. Mater. Interfaces* **2016**, *8*, 4000.
- [77] M.-S. Song, S.-C. Han, H.-S. Kim, J.-H. Kim, K.-T. Kim, Y.-M. Kang, H.-J. Ahn, S. X. Dou, J.-Y. Lee, *J. Electrochem. Soc.* **2004**, *151*, A791.
- [78] H. Tang, S. Yao, M. Jing, X. Wu, J. Hou, X. Qian, D. Rao, X. Shen, X. Xi, K. Xiao, *J. Alloys Compd.* **2015**, *650*, 351.
- [79] Y. Zhang, Y. Zhao, A. Yermukhambetova, Z. Bakenov, P. Chen, *J. Mater. Chem. A* **2013**, *1*, 295.
- [80] R. Yang, X. Song, M. Zhao, F. Wang, *J. Alloys Compd.* **2009**, *468*, 365.

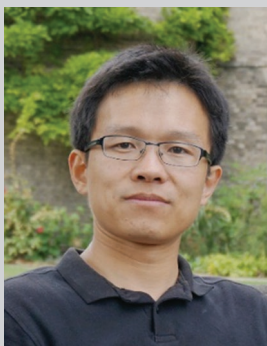
- [81] Y. Zhang, X. Wu, H. Feng, L. Wang, A. Zhang, T. Xia, H. Dong, *Int. J. Hydrogen Energy* **2009**, *34*, 1556.
- [82] T. Chen, X. Liu, L. Niu, Y. Gong, C. Li, S. Xu, L. Pan, *Inorg. Chem. Front.* **2020**, *7*, 567.
- [83] X. Liu, J. Q. Huang, Q. Zhang, L. Mai, *Adv. Mater.* **2017**, *29*, 1601759.
- [84] X. Cong, C. Cheng, Y. Liao, Y. Ye, C. Dong, H. Sun, X. Ji, W. Zhang, P. Fang, L. Miao, J. Jiang, *J. Phys. Chem. C* **2015**, *119*, 20864.
- [85] X. Tan, X. Wang, X. Wang, Y. Wang, C. Li, D. Xia, *Ionics* **2019**, *25*, 4047.
- [86] L. Wu, S. Tang, R. Qu, *J. Mater. Sci.: Mater. Electron.* **2019**, *30*, 189.
- [87] C. Dai, L. Hu, X. Li, Q. Xu, R. Wang, H. Liu, H. Chen, S.-J. Bao, Y. Chen, G. Henkelman, C. M. Li, M. Xu, *Nano Energy* **2018**, *53*, 354.
- [88] S. Li, P. Xu, M. K. Aslam, C. Chen, A. Rashid, G. Wang, L. Zhang, B. Mao, *Energy Storage Mater.* **2020**, *27*, 51.
- [89] X. Lu, Q. Zhang, J. Wang, S. Chen, J. Ge, Z. Liu, L. Wang, H. Ding, D. Gong, H. Yang, X. Yu, J. Zhu, B. Lu, *Chem. Eng. J.* **2019**, *358*, 955.
- [90] C. Yang, X. Wang, G. Liu, W. Yu, X. Dong, J. Wang, *J. Colloid Interface Sci.* **2020**, *565*, 378.
- [91] X. Liao, Z. Li, Q. He, L. Xia, Y. Li, S. Zhu, M. Wang, H. Wang, X. Xu, L. Mai, Y. Zhao, *ACS Appl. Mater. Interfaces* **2020**, *12*, 9181.
- [92] R. K. Bhardwaj, S. Jayanthi, P. S. Adarakatti, A. K. Sood, A. J. Bhattacharyya, *ACS Appl. Mater. Interfaces* **2020**, *12*, 28120.
- [93] J. Xiao, L. Wan, S. Yang, F. Xiao, S. Wang, *Nano Lett.* **2014**, *14*, 831.
- [94] X. Gao, Y. Wang, Z. Ma, W. Jiang, Y. Zou, C. Lu, *J. Mater. Sci.* **2016**, *51*, 5139.
- [95] H. Zhang, J. Liu, X. Lin, Y. Zhong, J. Ren, Z. Wang, T. Han, H. Li, *Ceram. Int.* **2020**, *46*, 14056.
- [96] H. Zhou, X. Li, Y. Li, M. Zheng, H. Pang, *Nano-Micro Lett.* **2019**, *11*, 40.
- [97] C. Zhang, J. J. Biendicho, T. Zhang, R. Du, J. Li, X. Yang, J. Arbiol, Y. Zhou, J. R. Morante, A. Cabot, *Adv. Funct. Mater.* **2019**, *29*, 1903842.
- [98] Y.-S. Liu, Y.-L. Bai, X. Liu, C. Ma, X.-Y. Wu, X. Wei, Z. Wang, K.-X. Wang, J.-S. Chen, *Chem. Eng. J.* **2019**, *378*, 122208.
- [99] D. Su, M. Cortie, H. Fan, G. Wang, *Adv. Mater.* **2017**, *29*, 1700587.
- [100] D. Morgan, A. V. Van der Ven, G. Ceder, *Electrochem. Solid-State Lett.* **2004**, *7*, A30.
- [101] G.-L. Xu, Q. Wang, J.-C. Fang, Y.-F. Xu, J.-T. Li, L. Huang, S.-G. Sun, *J. Mater. Chem. A* **2014**, *2*, 19941.
- [102] C.-S. Kim, A. Guerfi, P. Hovington, J. Trottier, C. Gagnon, F. Barray, A. Vijn, M. Armand, K. Zaghib, *Electrochem. Commun.* **2013**, *32*, 35.
- [103] J. Lee, J. Oh, Y. Jeon, Y. Piao, *ACS Appl. Mater. Interfaces* **2018**, *10*, 26485.
- [104] B. Wang, F. Jin, Y. Xie, H. Luo, F. Wang, T. Ruan, D. Wang, Y. Zhou, S. Dou, *Energy Storage Mater.* **2020**, *26*, 433.
- [105] Y. Chen, W. Zhang, D. Zhou, H. Tian, D. Su, C. Wang, D. Stockdale, F. Kang, B. Li, G. Wang, *ACS Nano* **2019**, *13*, 4731.
- [106] J. Duan, Y. Zou, Z. Li, B. Long, Y. Du, *J. Electroanal. Chem.* **2019**, *847*, 113187.
- [107] Z. Zeng, X. Liu, *Adv. Mater. Interfaces* **2017**, *5*, 1701274.
- [108] J. Guo, Y. Xu, C. Wang, *Nano Lett.* **2011**, *11*, 4288.
- [109] M. Liu, F. Ye, W. Li, H. Li, Y. Zhang, *Nano Res.* **2016**, *9*, 94.
- [110] Q. Pang, X. Liang, C. Y. Kwok, L. F. Nazar, *J. Electrochem. Soc.* **2015**, *162*, A2567.
- [111] G. Ardel, D. Golodnitsky, K. Freeman, E. Peled, G. B. Appetecchi, P. Romagnoli, B. Scrosati, *J. Power Sources* **2002**, *110*, 152.
- [112] J. Gao, M. A. Lowe, Y. Kiya, H. D. Abruña, *J. Phys. Chem. C* **2011**, *115*, 25132.
- [113] S. S. Zhang, *Front. Energy Res.* **2013**, *1*, 10.
- [114] Z. Zeng, X. Liu, *Adv. Mater. Interfaces* **2018**, *5*, 1701274.
- [115] A. Ghosh, A. Kumar, T. Das, A. Ghosh, S. Chakraborty, M. Kar, D. R. MacFarlane, S. Mitra, *Adv. Funct. Mater.* **2020**, 2005669.
- [116] J. Zheng, J. Tian, D. Wu, M. Gu, W. Xu, C. Wang, F. Gao, M. H. Engelhard, J.-G. Zhang, J. Liu, J. Xiao, *Nano Lett.* **2014**, *14*, 2345.
- [117] M. Waqas, S. Ali, D. Chen, B. Boateng, Y. Han, M. Zhang, J. Han, J. B. Goodenough, W. He, *Composites, Part B* **2019**, *177*, 107448.
- [118] M. Rana, B. Luo, M. R. Kaiser, I. Gentle, R. Knibbe, *J. Energy Chem.* **2020**, *42*, 195.
- [119] H. Wang, W. Zhang, J. Xu, Z. Guo, *Adv. Funct. Mater.* **2018**, *28*, 1707520.
- [120] Q. Pang, X. Liang, C. Y. Kwok, L. F. Nazar, *J. Electrochem.* **2015**, *162*, A2567.
- [121] F. Y. Fan, W. C. Carter, Y.-M. Chiang, *Adv. Mater.* **2015**, *27*, 5203.
- [122] M. F. Bell, J. A. Harrison, *J. Electroanal. Chem. Interfacial Electrochem.* **1973**, *43*, 305.
- [123] G. Gunawardena, G. Hills, I. Montenegro, B. Scharifker, *J. Electroanal. Chem.* **1982**, *138*, 255.
- [124] Q. Huang, H. Deligianni, L. T. Romankiw, *J. Electrochem.* **2016**, *153*, C332.
- [125] T. Zhou, W. Lv, J. Li, G. Zhou, Y. Zhao, S. Fan, B. Liu, B. Li, F. Kang, Q.-H. Yang, *Energy Environ. Sci.* **2017**, *10*, 1694.
- [126] T. Ling, P. Da1, X. Zheng, B. Ge, Z. Hu, M. Wu, X.-W. Du, W.-B. Hu, M. Jaroniec, S.-Z. Qiao, *Sci. Adv.* **2018**, *4*, eaau6261.
- [127] J. Wang, B. Wylie-van Eerd, T. Sluka, C. Sandu, M. Cantoni, X. K. Wei, A. Kvasov, L. J. McGilly, P. Gemeiner, B. Dkhil, A. Tagantsev, J. Trodahl, N. Setter, *Nat. Mater.* **2015**, *14*, 985.
- [128] M. R. Morris, S. R. Pendlebury, J. Hong, S. Dunn, J. R. Durrant, *Adv. Mater.* **2016**, *28*, 7123.
- [129] Y. Cui, J. Briscoe, S. Dunn, S. R. Pendlebury, J. Hong, S. Dunn, *Chem. Mater.* **2013**, *25*, 4215.
- [130] M. Rana, S. A. Ahad, M. Li, B. Luo, L. Z. Wang, I. Gentle, *Energy Storage Mater.* **2019**, *18*, 289.



**Yi-Cheng Jiang** received her B.S. in Chemistry from Sichuan University in 2015. She is currently a Master student majoring at Materials Science and Engineering at Nankai University, China. Her work focuses on seeking for advanced materials for a better lithium–sulfur rechargeable battery.



**Hafiz Muhammad Umair Arshad** earned his B.S. (Hons.) degree in Physics from the G.C. University Faisalabad and M.S. degree in Physics from the University of Agriculture Faisalabad, Pakistan in 2013 and 2015, respectively. Currently, He is a Ph.D. student in School of Material Science and Engineering, Nankai University, China. His current research interests focus on the design, development of effective strategies, and application of the advanced cathode materials for high energy and long-life lithium–sulfur battery.



**Guo-Ran Li** is a professor in Material Chemistry at School of Materials Science and Engineering, Nankai University, China. His main current research interest is the study of new energy materials and devices, and in particular for rechargeable batteries and hybrid solar cells. He received a Bachelor's degree in Chemistry and a Ph.D. degree in Physical Chemistry in 2000 and 2005, both from Nankai University. He worked as Endeavour Australia Cheung Kong Research Fellow in Queensland University of Technology in 2008, and as a visiting researcher at University of Cambridge from 2014 to 2015.



**Xue-Ping Gao** is a professor at the Institute of New Energy Material Chemistry, Nankai University of China. He received his doctorate at Department of Chemistry from Nankai University in 1995. He worked as a visiting research fellow at Kogakuin University in Japan from 1997 to 1999. Currently, his main research focuses on energy storage materials for power sources, including Li-ion batteries, Li–S battery, and solar rechargeable battery.